Biochemical Characterization of *Aspergillus fumigatus* SidA: A Flavin-Dependent N-hydroxylating Enzyme

Samuel Wyatt Chocklett

Thesis submitted to the faculty of

Virginia Polytechnic Institute and State University

in partial fulfillment of the requirements for the degree of

Master of Science in Life Sciences

In

Biochemistry

Pablo Sobrado, Chair

Dennis R. Dean

Erin L. Dolan

December 9, 2009

Blacksburg, Virginia

Keywords: *Af* SidA, hydroxylation, *Aspergillus fumigatus*, flavin, siderophore

Biochemical Characterization of *Aspergillus fumigatus* SidA: A Flavin-Dependent N-hydroxylating Enzyme

Samuel Wyatt Chocklett

Pablo Sobrado, Chair

ABSTRACT

Ferrichrome is a hydroxamate-containing siderophore produced by the pathogenic fungus *Aspergillus fumigatus* during infection. This siderophore includes N^5-hydroxylated L-ornithine in the peptide backbone that serve as iron chelators. *Af* SidA is the L-ornithine N^5-hydroxylase, which performs the first enzymatic step in the biosynthesis of ferrichrome. In this study, *Af* SidA was recombinantly expressed and purified as a soluble tetramer with a bound FAD cofactor. The enzyme demonstrated typical Michaelis-Menten kinetics in a product formation assay with respect to L-ornithine, but similar experiments as a function NADH and NADPH indicated inhibition at high coenzyme concentrations. *Af* SidA is highly specific for its substrate; however, it is promiscuous with respect to its coenzyme requirement. A multi-functional role of NADPH is observed since $NADP^+$ is a competitive inhibitor with respect to NADPH and steady-state kinetic experiments indicate that *Af* SidA forms a ternary complex with $NADP^+$ and L-ornithine for catalysis. Furthermore, in the absence of substrate, *Af* SidA forms a stable C4a-(hydro)peroxyflavin intermediate that is stable on the second time scale. *Af* SidA is also inhibited by several halides and the arginine-reactive reagent, phenylglyoxal. Biochemical comparison of *Af* SidA to other flavin-containing monooxygenases reveal that *Af* SidA likely proceeds by a sequential-ordered mechanism.

ACKNOWLEDGEMENTS

I would like to thank my advisor, Dr. Pablo Sobrado, for his encouragement, guidance, and patience during my graduate research tenure. His attention to detail, critical reasoning, and work ethic are the most valuable lessons I have learned during the years I spent in his laboratory.

I am very grateful to the members of my graduate committee, Dr. Dennis R. Dean and Dr. Erin Dolan, for their time, patience, and advice for the improvement of my research efforts. I would also like to thank the faculty members who served during my preliminary examination, Dr. David R. Bevan, Dr. Peter J. Kennelly and Dr. Marcy Hernick, for their support and valuable suggestions.

My deep appreciation goes to Valerie L. Cash for her support, patience and advice. Her source of knowledge, wisdom, and a variety of chemical supplies and equipment made possible many experiments in the laboratory.

I am also indebted to the past and present members of the Sobrado Laboratory: Jenna Hess, Anthony Irwin, Janice Llanos-Velázquez, Reeder Robinson, and Britni Souther; thank you for your friendship and assistance with many of the initial phases of my research. I extend my most sincere gratitude to my colleague, Michelle Oppenheimer, who repeatedly provided valuable input and assistance during experiments, while offering friendship during difficult times.

Last but not least, I thank my parents for their love and never-ending belief in my abilities. And, most especially, I would like to thank Pia Landis, whose love and support made this journey possible.

TABLE OF CONTENTS

LIST OF FIGURES

LIST OF TABLES

CHAPTER ONE

Introduction

1.1 Iron and activated oxygen species in biology

Living organisms have selected iron to achieve a large number of biological processes (Table 1.1) [1]. Iron's biochemical importance stands out because of its chemical versatility. Since iron can serve as both an electron acceptor and donor, the electronic versatility of iron allows it to occupy several valence states, ranging from zero-valent iron, Fe^{0}, up to Fe^{6+}. This permits iron to form a series of oxyanions, many of which are chemically and biologically active. The unique stability of iron comes from the extreme variability of the Fe^{2+}/ Fe^{3+} redox potential, which can be finely tuned by well-chosen ligands.

Iron in its various oxidation states plays critical roles. The most well-known utilization of iron is in oxygen transport in the red blood cells of vertebrates and in tissues of some invertebrates [2]. Here, iron is incorporated into a heme cofactor of hemoglobin, which binds molecular oxygen. Hemoglobin then transports oxygen from the lungs or gills to the rest of the body where it releases the oxygen for cell use. Similarly, iron is found in the heme cofactor of cytochrome P450 enzymes, which can metabolize thousands of endogenous or exogenous compounds, critical for the activation and degradation of a variety of toxic compounds [3]. Iron is also utilized in the heme cofactor of catalase, an enzyme used to breakdown deleterious hydrogen peroxide into water and molecular oxygen [4, 5]. Furthermore, iron can serve as the cofactor in Fe-superoxide dismutase, an antioxidant mechanism against all cells exposed to molecular oxygen [6-8]. Interestingly, iron complexes can also react with molecular oxygen or with

its reduced species, leading to highly reactive high-valent iron-oxo species. Here, multicomponent protein complexes are capable of activating O_2 molecules to initiate the degradation process of many biological contaminants and pollutants [9-11].

From the examples mentioned above, it is quite apparent that elemental iron is essential for life. As complex organisms, humans utilize a combination of these iron-dependent molecules and proteins to optimize function and viability. However, Fe^{3+} is not "free," but quickly oxidizes in aerobic environments, forming insoluble hydroxides, $(FeOH)_3$. As a result, the concentration of Fe^{3+} in water is very low (10^{-18} M) [12]. Mammalian iron-binding proteins such as hemoglobin and transferrin further reduce its concentration to an estimated 10^{-24} M in human serum [13]. For humans, this is advantageous since iron rapidly reacts with oxygen forming radicals, which can lead to DNA and protein damage.

This scarcity of available iron presents a predicament for bacterial cells, which require a cytoplasmic iron concentration of 10^{-6} M for growth [14]. To maintain iron homeostasis, many microbes use a variety of techniques to traffic elemental iron from the environment and extracellular spaces. Such examples include the import of iron from the mammalian iron carriers heme and transferrin or the production of low molecular weight molecules with high affinity for Fe^{3+} known as siderophores. As a result, these pathways involved in iron uptake have created new avenues of biochemical research with a direct impact on global health. Better comprehension of the complex machinery involved in iron trafficking by microorganisms can potentially lead to new therapeutic strategies against several of the world's deadliest diseases.

Table 1.1 Redox chemistry of iron and oxygen species.

Oxidizing Agent	Exchanged e^-	Reaction	Example
Ferrous iron as a reducing agent			
O_2	1	$LFe(II) + O_2 \longrightarrow LFe(III) + \dot{O}_2^-$	Autoxidation
O_2	3	$LFe(II) + O_2 \xrightarrow[e^-]{2H^+} {}^{+}LFe(IV)=O + H_2O$ $\updownarrow$ $LFe(V)=O$	Cyt P450
$\dot{O}_2^-$	1	$LFe(II) + \dot{O}_2^- \xrightarrow{2H^+} LFe(III) + H_2O_2$	Iron SOD (step 2)
H_2O_2	1	$LFe(II) + H_2O_2 \longrightarrow LFe(III) + HO^- + HO^\bullet$	Fenton reaction
H_2O_2	2	$LFe(II) + H_2O_2 \longrightarrow LFe(IV)=O + H_2O$	Fe-EDTA
Ferric iron as a reducing agent			
H_2O_2	2	$LFe(III) + H_2O_2 \longrightarrow {}^{+}LFe(IV)=O + H_2O$ $-H^+ \downarrow$ $\quad$ $+H^+ \uparrow$ $\quad \downarrow$ $LFe(III)\text{-}O\text{-}O\text{-}H \qquad LFe(V)=O$	Catalases Peroxidases
Superoxide as a reducing agent			
$LFe(III)$	1	$\dot{O}_2^- + LFe(III) \longrightarrow O_2 + LFe(II)$	Iron SOD (step 1) Haber-Weiss (step 1)
Hydrogen peroxide as a reducing agent			
H_2O_2	2	$H_2O_2 + LFe(V)=O \longrightarrow H_2O + O_2 + LFe(III)$	Catalases
D (Nucleophile) as a reducing agent			
$LFe(IV)=O$	1	$\ddot{D} + LFe(IV)=O \xrightarrow{2H^+} \dot{D} + H_2O + LFe(III)$	Peroxidases
$LFe(IV)=O$	1	$\ddot{D} + {}^{+}LFe(IV)=O \longrightarrow D + LFe(IV)=O$	Peroxidases
$\updownarrow$ $LFe(V)=O$	2	$\ddot{D} + LFe(V)=O \longrightarrow DO + LFe(III)$	Monooxygenases

L: ligand; D: nucleophile.

1.2 Iron acquisition

1.2.1 Iron-specific transport and assimilation

Most organisms depend on the availability of iron for growth, with notable exceptions including the bacteria *Borrelia burgdorferi* and *Lactobacillus plantarum* [15, 16]. Therefore, many bacteria and fungi have evolved various strategies, often used in parallel, to acquire iron for metabolic processes. It is documented, for example, that the fungus *Aspergillus fumigatus* uses a combination of systems to acquire iron: (*i*) ferrous iron uptake, (*ii*) reductive iron assimilation, and (*iii*) siderophore-mediated iron uptake [17]. The fact that *A. fumigatus* has developed several iron acquisition strategies is likely a result of the organism's ability to adapt and proliferate in numerous environments.

On the other hand, some organisms only require a single iron acquisition system. For example, *Helicobacter pylori*, the causative agent of type B gastritis, relies on a Fe^{2+}/ Fe^{3+} iron uptake system for survival in the low pH, low-O_2 environment of the human stomach [18]. In one study, Blaser and co-workers created a series of mutant strains of *H. pylori* lacking specific Fe^{2+}/ Fe^{3+} citrate transporters based upon the known genome sequence. It was demonstrated that inactivation of the iron acquisition gene, *feoB*, resulted in ~10-fold lower iron transport than the wild-type, regardless of whether iron was supplied in its ferric or ferrous forms. Moreover, growth inhibition in iron-deficient media in this mutant was only relieved when cells were supplemented with holo-transferrin, holo-lactoferrin, and Fe^{3+} dicitrate. It was not until complementation of the *feoB* mutant that full Fe^{2+} and Fe^{3+} transport was fully restored [19].

In support of Blaser's findings, Suzuki and co-workers constructed a *Magnetospirillum magneticum* knockout of ORF4, encoding a putative cytoplasmic

ATPase [20]. Here, it was presented that iron trafficking through the cytoplasmic membrane was dependent on the gene product of ORF4 and therefore the ability of the *M. magneticum* mutant to take up iron was severely compromised. Also, ferrous iron concentration in the medium decreased more with the wild-type strain than the mutant and the iron content in the cytoplasmic fraction of the mutant was much lower than the wild-type strain [20]. Together, these findings indicate that iron acquisition by specific iron uptake systems relying on iron-specific receptor proteins serve as one possible pathway for microbial iron homeostasis.

Reductive iron assimilation, the sequestration and subsequent reduction of elemental iron (e.g., Fe^{3+} to Fe^{2+}) for later storage, serves as an alternative method for iron acquisition in many organisms. It is important to note, however, that each system is not an absolute requirement for survival. In fact, Schrettl and co-workers studied the effects of deletions in the various iron acquisition systems in *A. fumigatus* to demonstrate the adaptability of this highly opportunistic pathogen [17]. To test the requirement for the reductive iron assimilation gene (Δ*ftrA*) in a murine model, a comparison was performed between the virulence of the wild-type strain and the otherwise isogenic Δ*ftrA* strain. Groups of mice were intranasally inoculated with doses (2×10^5 conidiospores) of each strain. The Δ*ftrA* mutant strain was as virulent as the wild-type, demonstrating that reductive iron assimilation has little to no role in *A. fumigatus* virulence.

1.2.2 Siderophore-mediated iron acquisition

In contrast to iron-specific receptors and transporters, many invasive intracellular pathogens, such as *Mycobacterium tuberculosis*, *Aspergillus fumigatus*, *Bacillus*

anthracis, *Yersinia pestis*, and *Escherichia coli*, obtain iron via an indirect process involving the synthesis, secretion, and reuptake of small molecule iron chelators, under iron-limiting conditions, termed siderophores [21-23]. Siderophores are structurally diverse and contain a mixture of hydroxamates, catechols, carboxylates or phenols for iron coordination. *E. coli* synthesize the prototypical aryl-capped siderophore enterobactin, while *M. tuberculosis* synthesize the mycobactins (Figure 1.1).

Many species of gram-negative enteric bacteria such as *E. coli*, contain a ~24 kb gene cluster encoding thirteen proteins that collaborate to synthesize, transport and process their respective siderophores. For example, after the assembly of enterobactin, the siderophore can compete successfully for Fe^{3+} binding against all known protein and small molecule ligands, given its remarkably strong affinity for Fe^{3+} ($K_D = 10^{-49}$ M) [24]. The Fe^{3+}- enterobactin complex is then imported through the outer-membrane enterobactin-specific porin FepA, escorted through the periplasm by FepB and pumped through the two-protein inner-membrane channel FepDG into the cytoplasm by FepC-catalyzed ATP hydrolysis [25-27]. Liberation of Fe^{3+} from enterobactin requires enzymatic degradation of its trilactone scaffold to three equivalents of DHB-Ser by the esterase Fes before the tightly sequestered ferric iron can be transferred to intracellular iron carriers [28]. The entire enterobactin system is under transcriptional control by the iron-dependent repressor, Fur, which serves as a sensor for intracellular iron by dissociating from its DNA-binding site when iron is scarce. Therefore, transcription of the enterobactin synthesis, export and import genes is activated during low-iron conditions and repressed when iron is abundant [12, 29].

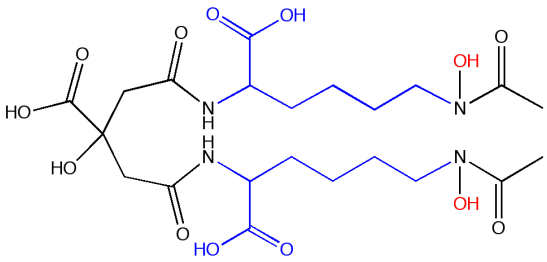

Aerobactin (*Escherichia coli*)

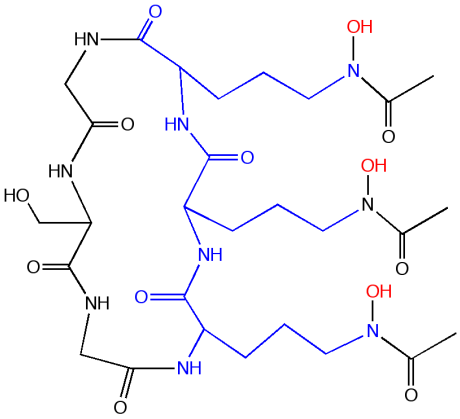

Ferrichrome (*Aspergillus fumigatus*)

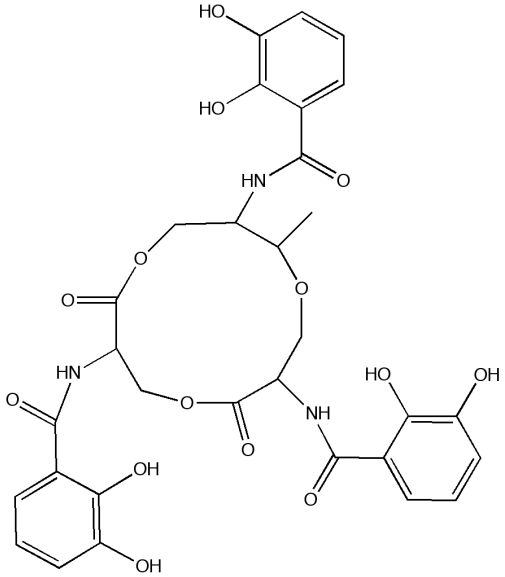

Enterobactin (*Escherichia coli*)

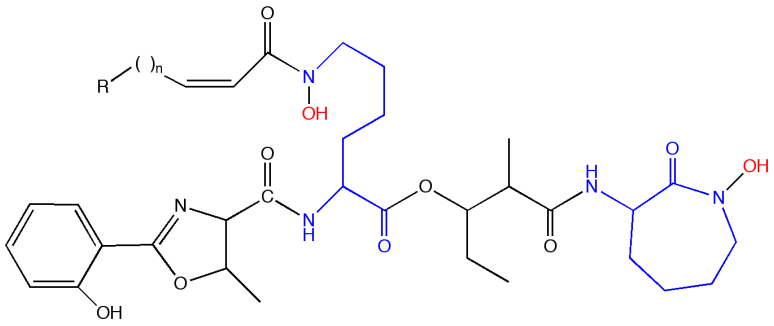

Mycobactin (*Mycobacterium tuberculosis*)

Figure 1.1. Chemical structures of siderophores.

1.3 Siderophore biosynthesis

1.3.1 General characteristics

Siderophore biosynthesis has been under recent review as an alternative route for antibiotic development against multi-drug resistant pathogens. These intense investigations have revealed two operationally different mechanisms. The best understood is the thio-templated assembly process catalyzed by nonribosomal peptide synthetases (NRPSs) sometimes in conjunction with polyketides synthases, wherein the biosynthetic chain intermediates remain attached to carrier domains during assembly [30]. Additionally, many carboxylate- and hydroxamate-containing siderophores such as aerobactin are synthesized by a non-templated route, utilizing freely diffusible biosynthetic intermediates [31].

As expected, there are inherent differences among the siderophore biosynthetic pathways. Despite these differences, the mechanisms of siderophore biosynthesis follow the same fundamental enzymatic logic, which involves a series of elongating siderophore intermediates on multimodular protein assembly lines. A substantial variety of siderophore structures are produced from similar NRPS assembly lines. In fact, variation can come in the choice of the phenolic acid selected as the *N*-cap, the modification of amino acid residues during chain elongation, the mode of chain termination, and the nature of the capturing nucleophile of the siderophore acyl chain being released. The specific parts that get assembled in a given bacterium may reflect a combination of the inventory of biosynthetic and tailoring gene clusters available. This modular assembly logic can account for many known siderophores [22].

1.3.2 Hydroxamate-containing siderophores

To date, several hundred siderophores have been isolated and characterized that vary considerably in chemical composition. In contrast to enterobactin, a separate class of amphiphilic, hydroxamate-containing siderophores has recently been discovered [32]. This class of siderophore, with such examples as mycobactin (*M. tuberculosis*) and ferrichrome (*A. fumigatus*), are unique in that they incorporate freely diffusible amino acid substrates into the backbone of the siderophore. It has been demonstrated that once mature, these siderophores not only confer virulence, but are also required for resistance to oxidative stress, asexual/sexual development, iron storage and protection against iron-induced toxicity in some organisms [33].

The biosynthesis of the phenolic-containing siderophore enterobactin involves condensation, acylation and cyclization. However, the exact nature by which the hydroxamate siderophores are synthesized is not as clear. Currently, there are two proposed models by which hydroxamate siderophores are produced, which differ in the final assembly of the macromolecule. Specifically, it has been proposed that depending on the organism, that hydroxamate-containing siderophores are synthesized either through the linking of several peptidic fragments or through the successive condensation of subunits onto a single attachment location [34]. Depending on the organism, many microbes produce more than one siderophore, including specific intra- and extracellular forms. Because the individual steps of siderophore biosynthesis from a single organism can vary greatly, it is difficult to assign a single enzyme to multiple pathways.

Although biosynthetic pathways can differ even within a single microbe, many hydroxamate-containing siderophores depend on the action of a flavin adenine

dinucleotide (FAD)-dependent monooxygenase, which performs the first enzymatic step in the biosynthetic pathway. This enzyme consumes NADPH and molecular oxygen to insert a single oxygen atom onto the terminal amino group of either L-lysine or its one-carbon derivative L-ornithine. The product from this reaction, containing a hydroxylated amine, is then incorporated into the backbone of the siderophore, thereby allowing the hydroxyl to directly coordinate ferric iron (Figure 1.2). Additionally, this enzyme is utilized multiple times during siderophore biosynthesis (Figure 1.1). For example, three molecules of L-ornithine are converted to their hydroxy-derivatives during ferrichrome biosynthesis.

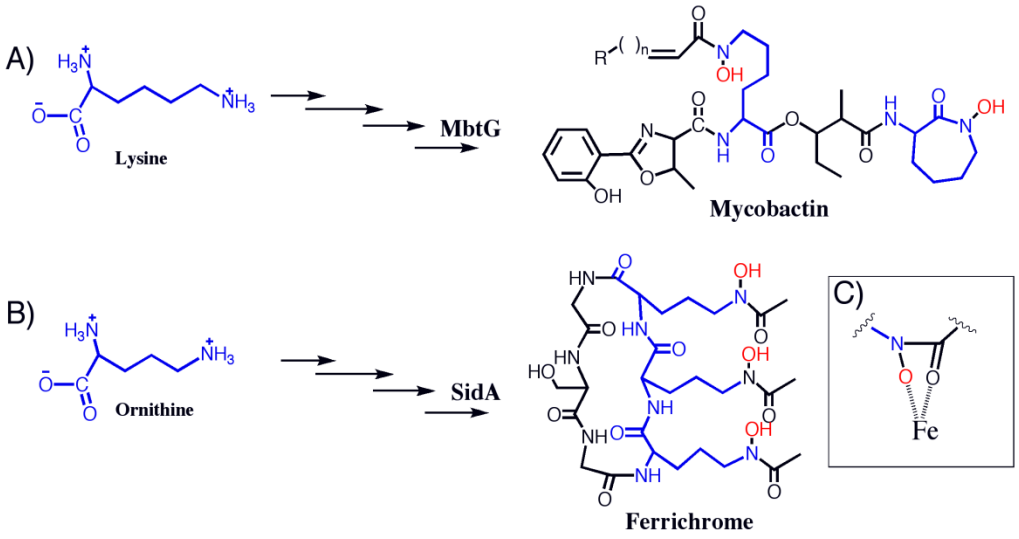

Figure 1.2. Amino acid incorporation into hydroxamate-containing siderophores. MbtG and *Af* SidA are flavoprotein monooxygenases that utilize FAD and NADPH as cofactors to convert L-lysine to Lys-N^6-OH or L-ornithine to Orn-N^5-OH. The products of these reactions are then incorporated into the backbone of the hydroxamate-based siderophores, mycobactin **(A)** or ferrichrome **(B)**. Upon maturation, these siderophores properly coordinate ferric iron by means of their hydroxyl and keto-functional groups **(C)**.

1.4 Diseases associated with siderophore production and utilization

The ability of many pathogens to grow in their respective hosts, especially in iron-limited extracellular spaces such as respiratory cavities, is dependent, in part, on their ability to scavenge iron. Like many other pathogens, *M. tuberculosis* and *A. fumigatus* synthesize and secrete siderophores and then specifically take up those complexed with iron to meet their biological needs.

M. tuberculosis, the etiological agent of tuberculosis (TB) and *A. fumigatus*, the causative agent of invasive aspergillosis (IA), are pathogens with serious impacts on global public health. According to the World Health Organization, an estimated 1.6 million deaths resulted from tuberculosis infections in 2005 alone [35]. Moreover, multidrug-resistant (MDR) tuberculosis is an emerging pandemic and the surfacing of extensive drug-resistant (XDR) tuberculosis poses a new global threat [36, 37]. To complicate matters, TB treatments require an intense regimen of antibiotics for up to six months, which includes an inhibitor "cocktail" of isoniazid, rifampicin, pyrazinamide, and ethambutol. Even still, there is a 2 – 3% relapse occurrence with this treatment.

IA is the most common cause of death due to fungal infections, occurring in up to 25% of transplant recipients or patients undergoing therapy for hematological malignancies, and 3% of AIDS patients [38]. Typically, mortality associated with this disease reaches up to 100%, due to difficulties with diagnosis and treatment [39]. Allergic bronchiopulmonary aspergillosis, an *A. fumigatus*-induced respiratory disease usually found in hypersensitive individuals, can be life threatening and frequently occurs in patients suffering from bronchial asthma, bronchiectasis, or cystic fibrosis [40, 41]. In the United States in 1996, the cost of treating diagnosed cases of IA was estimated at

$633 million, with each case costing approximately $64,500 [42]. Currently, there are only two effective antifungal treatments against IA, amphotericin B and the slightly less effective itraconazole. At best, repeated doses of amphotericin B has only yielded marginal benefit in some cases [43]. Because humans do not produce siderophores, these iron chelators represent a new avenue for antibiotic development. Therefore, it is essential to characterize the siderophore biosynthetic machinery to assist in the development of new therapeutic strategies against several deadly pathogens, notably *M. tuberculosis*, *Y. pestis*, and *A. fumigatus*.

1.5 L-ornithine N^5-oxygenase as a novel drug target

It is clear that historically effective treatments against many diseases through the inhibition of DNA replication, cell wall formation and protein synthesis are, and will continue to be, ineffective against MDR pathogens. Therefore, a new methodology for the treatment of these deadly diseases is urgently needed. In response, there are laboratories currently investigating the inhibition of siderophore biosynthesis via an enzyme-specific, mechanism-based approach. For example, Quadri and co-workers recently investigated the inhibition of *M. tuberculosis* and *Y. pestis*, the causative agent of the plague [44]. Their experimental rationale was to design small-molecule inhibitors that block siderophore biosynthesis and as a result, bacterial growth and virulence under iron-limiting conditions. These inhibitors would be powerful tools for elucidating the relevance of siderophores at specific stages of infection because they could be used to provide active control of siderophore production in animal models of bacterial infection [44].

During the biosynthesis of *M. tuberculosis* siderophores (MBTs) and *Y. pestis* siderophores (YBTs), the domain salicylation enzymes, MbtA and YbtE, catalyze the salicylation of an ArCP domain through a two-step reaction [32]. These enzymes are homologous to EntE in enterobactin biosynthesis and catalyze the initial reaction in MBT and YBT biosynthesis. Because MbtA and YbtE have no homologs in humans, they are particularly attractive targets for the development of antibiotics that inhibit siderophore biosynthesis [44]. Extensive studies lead to the discovery that the inhibitor 5'-O-(*N*-salicylsulfamoyl) adenosine (salicyl-AMS) lead to the inhibition of salicylate adenylation activity in both MbtA and YbtE. Furthermore, siderophore production assays showed that salicyl-AMS decreased MBT production to virtually undetectable levels and YBT production was inhibited by approximately five-fold relative to controls [44]. Thus, salicyl-AMS is a promising initial lead compound for the development of new antibiotics to treat tuberculosis and the plague.

Logically, only those enzymes essential for siderophore biosynthesis are the most promising candidates as drug targets. As a result, Schrettl and co-workers demonstrated that the L-ornithine N^5-oxygenase in *A. fumigatus,* was required for both siderophore production and virulence [38]. To test the requirement for siderophore-mediated iron acquisition in *A. fumigatus,* a mutant strain with a deletion of the *Af sidA* gene was constructed. Infection in a murine model was performed between the wild-type strain and the otherwise isogenic Δ*sidA* strain, identical to their Δ*ftrA* mutant strain study. In contrast to the Δ*ftrA* mutant strain, mice inoculated with the Δ*sidA* mutant demonstrated only modest weight loss and all those infected survived to the conclusion of the experiment. Reconstruction of *Af sidA* resulted in restoration of virulence to wild-type

levels, demonstrating that the *Af sidA* gene is absolutely required for *A. fumigatus* virulence. Furthermore, knockout mutants of the L-ornithine N^5-oxygenases in *Pseudomonas aeruginosa* and *Burkholderia cepacia* lead to attenuation of virulence in these organisms because of their inability to synthesize siderophores [45-47]. Because these L-ornithine N^5-oxygenases are required for siderophore production and thus, virulence, current research focuses on their biochemical and structural characterization for possible therapeutic uses.

1.6 *Af* SidA is a flavin-dependent N-hydroxylating enzyme

Af SidA catalyzes the hydroxylation of the terminal amino group of L-ornithine. The product of this reaction is then directly coordinated into the backbone of the *A. fumigatus* hydroxamate siderophore, ferrichrome (Figure 1.2). The action of this enzyme requires the use of a widely distributed biological cofactor, flavin adenine dinucleotide (FAD, Figure 1.3). Flavoproteins are unique as biological catalysts in that they carry out a wide variety of different biochemical processes. The redox capability of FAD allows this cofactor to participate in a variety of reactions, including bioluminescence, dehydrogenation, halogenation, isomerization, and oxygenation activation [48-53]. In these reactions, the flavin cofactor exists in different redox states and its biochemical role involves changing between these states. Moreover, access to these redox states allows flavoproteins to participate in one-electron transfer and two-electron transfer reactions. As a result, this capability sets FAD apart from enzymes which use other coenzymes, like pyridine nucleotides, pyridoxal phosphate or thiamin pyrophosphate, each of which involves a single type of chemical event [54].

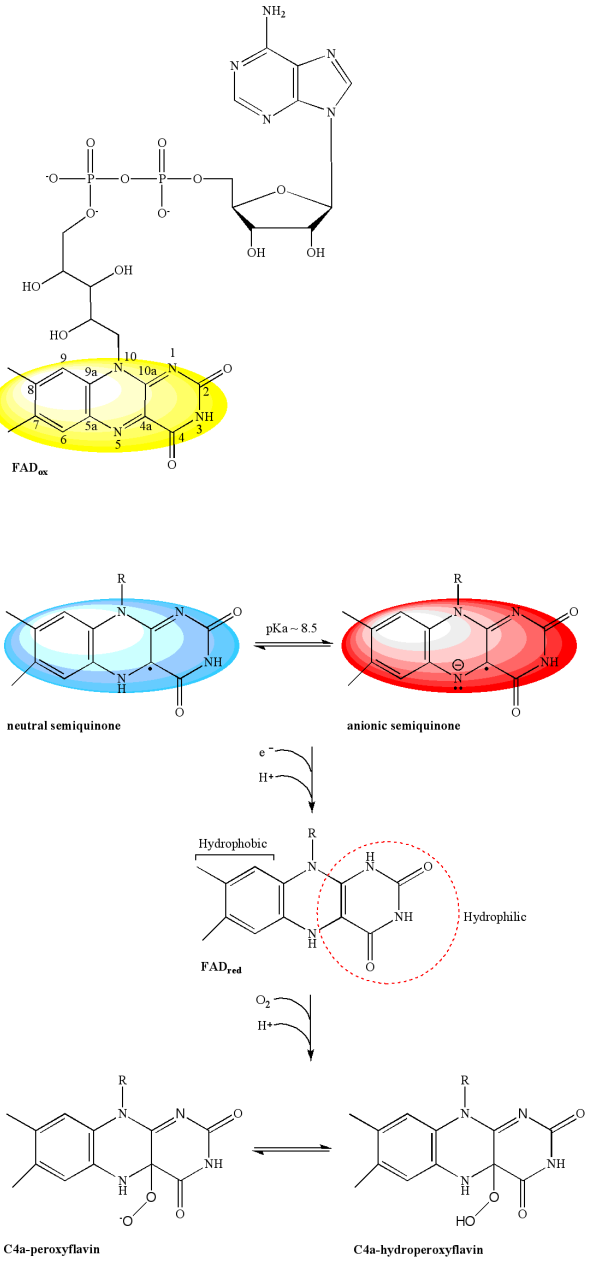

Figure 1.3. The chemical reactivity of FAD. Oxidized FAD (*yellow*) can undergo a one-electron transfer reaction, yielding the neutral semiquinone (*blue*) or at high pH, the anionic semiquinone (*red*). A second one-electron transfer to FAD yields the fully reduced cofactor (*white*). Upon reduction, FAD reacts with molecular oxygen, forming either the unprotonated C4a-peroxyflavin or the protonated C4a-hydroperoxyflavin.

FAD is derived from riboflavin (vitamin B_2). It consists of a riboflavin group bound to the phosphate group of an adenosine diphosphate molecule. Chemically, the most important constituent of the flavin cofactor is the isoalloxazine ring. This three-member ring is the location of electron transfer during redox reactions, as well as a site for amino acid side chain binding. Although most flavoproteins contain a non-covalently bound FAD (or FMN) cofactor, a large number have FAD covalently linked to the polypeptide chain. Most covalent flavin-protein linkages involve a single attachment via a histidyl, tyrosyl, cysteinyl or threonyl residue. However, some flavoproteins involve linkages with a combination of two of these amino acids [55]. The variety of flavin-dependent enzymes is due to the interaction of the isoalloxazine ring with the protein, which requires fine tuning by well-chosen ligands. The isoalloxazine ring is amphipathic: the xylene moiety is hydrophobic and prone to interact with hydrophobic protein areas, whereas the pyrimidine ring is relatively electron-deficient and hydrophilic, and is comparable with pyrimidine bases in its ability to form hydrogen bridges [54].

The study of the various oxidation states of the isoalloxazine ring of FAD is an important diagnostic tool in the assignment of a kinetic mechanism to a specific flavoprotein. As mentioned, FAD undergoes changes in its oxidation state during catalysis. Specifically, the flavin cofactor can adopt one of three redox states: fully oxidized, an intermediate semiquinone, or fully reduced. In each of these states, its chemical properties are markedly different, particularly the isoalloxazine ring. As shown in Figure 1.3, oxidized FAD absorbs visible light in the 350 – 450 nm range, giving it a characteristic bright yellow color. Oxidized FAD is converted to a semiquinone by a one-electron transfer. At physiological pH, the semiquinone is a neutral radical and is

blue in color, with a λ_{max} of 570nm and p*K*a of about 8 – 8.5 [56]. When the semiquinone loses a proton at higher pH values, it becomes a radical anion, displaying a red color with a λ_{max} of 490 nm. This FAD intermediate is particularly stable, owing to extensive delocalization of the unpaired electron across the π – electron system of the isoalloxazine ring system. A second one-electron transfer converts the semiquinone to the completely reduced $FADH_2$, at which point color is lost or "bleached" [57].

Once fully reduced, the versatility of the flavin cofactor is apparent. In the case of flavoprotein monooxygenases, the major common property is the use of reducing equivalents for reduction of the flavin and the formation of a C4a-hydroperoxyflavin on reaction of the reduced enzyme with molecular oxygen; this is the reactive oxygen species that is responsible for oxygenation of the substrate [53]. The anionic peroxyflavin is a good nucleophile and forms initially upon reaction with molecular oxygen. This flavin intermediate is responsible for the oxygen-insertion reactions catalyzed by Bayer-Villiger monooxygenases. On the other hand, the peroxyflavin can also become protonated, forming the hydroperoxyflavin, a strong electrophile. This flavin intermediate is responsible for a series of hydroxylation reactions. Therefore, reaction of the reduced flavin with molecular oxygen provides this cofactor with the capability to catalyze a diverse range of reactions.

It is the intent of this study to discuss the biochemical characterization of *Aspergillus fumigatus* SidA. Specifically, emphasis will be placed on the recombinant expression and purification of the protein, the steady-state kinetic parameters, oxygenated flavin intermediates, conformational changes induced during catalysis and, finally, small molecule inhibition of the enzyme.

CHAPTER TWO

Cloning, Expression, and Purification of *Af* SidA

I. Introduction

Current therapeutics against many deadly diseases, including TB and aspergillosis are focused on the development of enzyme-specific inhibitors against siderophore biosynthesis. Recently, work has also been applied to the understanding of particular enzymes involved in siderophore biosynthesis where amino acid substrates are incorporated into the siderophore backbone. One such example is the utilization of L-ornithine by flavin-dependent N-hydroxylating monooxygenases (NMOs, Figure 1.2). Several L-ornithine N^5-oxygenases have been identified, yet only PvdA (*P. aeruginosa*), VbsO (*Rhizobium etli* CFN42) and CchB (*Streptomyces coelicolor*) have been purified and enzymatically investigated [34, 58-60]. However, biochemical characterization of these NMOs has been hindered due to the lack of a bound FAD cofactor upon purification. In fact, it was shown that FAD is an obligatory participant in each reaction and a concentration of ~ 50 μM FAD was added to the reaction mixture to ensure activity. Furthermore, there is no three-dimensional structure for any member of the NMOs. Thus, obtaining purified preparations of these enzymes with a bound FAD cofactor will assist in the detailed biochemical and structural characterization of this class of flavoprotein monooxygenases.

In this chapter, the cloning, recombinant expression, and purification of the L-ornithine N^5-oxygenase from the pathogenic fungus *Aspergillus fumigatus* is reported (*Af* SidA). *Af* SidA was chosen for this study based upon several criteria: (*i*) the genome sequence of *Aspergillus fumigatus* is known, (*ii*) the gene product of *Af sidA* is shown to

be essential for siderophore production, as well as virulence, and (*iii*) *Af* SidA currently lacks any biochemical or structural characterization.

II. Materials and Methods

2.2.1 Materials

DNA encoding the *A. fumigatus* strain *Af*293 *sidA* gene, ligated into the pUC57 plasmid, was obtained from GenScript Corporation (Piscataway, NJ). Enzymes used in cloning and limited proteolysis were from Promega Corporation (Madison, WI). *E. coli* TOP10 and BL21T1^{R} chemically competent cells were from Invitrogen and the pVP55A and pVP56K plasmids were obtained from the Fox Laboratory (University of Wisconsin-Madison). DNA sequencing was performed at the Virginia Bioinformatics Institute DNA Sequencing Facility. Protein purification was performed on an ÄKTA Prime FPLC system (GE Healthcare). L-lysine, L-ornithine, substrates and inhibitors, as well as buffers and salts, were purchased from ThermoFisher Scientific and used without further purification.

2.2.2 Cloning of *Aspergillus fumigatus sidA*

DNA encoding the *Af sidA* gene was flanked by the restriction cut site SgfI at the 5' end and PmeI at the 3' end. The pUC57 plasmid containing the *Af sidA* gene was directly transformed into *E. coli* TOP10 cells. Colonies were screened for the presence of the *Af sidA* insert by digestion with Flexi® enzyme blend (SgfI and PmeI). The Flexi® cloning system is a simple, yet powerful directional cloning method for protein-coding sequences. It is based on two rare-cutting restriction enzymes, SgfI and PmeI. First, sites

for these enzymes are added to the ends of the protein-coding region of interest. Next, the protein-coding region is amplified using two primers, one containing a SgfI site, the other containing a PmeI site. As a result, the purified PCR product contains the protein-coding region and both SgfI and PmeI restriction sites. The liberated gene was ligated into similarly treated pVP55A and pVP56K expression plasmids to generate either a *His_8-sidA* or *His_8-mbp-sidA* construct, respectively. DNA sequencing confirmed the presence of the desired gene and the *pVP55A:sidA* or *pVP56K:sidA* plasmids were transformed into *E. coli* BL21T1^R cells for subsequent protein expression.

2.2.3 Heterologous expression and purification of His_8-MBP-*Af* SidA

Due to the insolubility of the *His_8-Af sidA* gene product, subsequent expression methods utilized the *pVP56K:sidA* expression plasmid, which expresses *Af sidA* as a fusion to maltose binding protein (MBP). An overnight culture of BL21T1^R cells containing the *pVP56K:sidA* plasmid was used to inoculate six 1.5-L flasks of Luria-Burtani (LB) broth supplemented with kanamycin (100 µg/ml). Cultures were grown with shaking at 37^{o}C to an OD_{600} ~ 0.6. For induction, 150 µM isopropyl-β-D-1-thiogalactopyranoside was added aseptically. After four hours of induction, cells were harvested by centrifugation and stored at -80^{o}C. Cells were resuspended in buffer A (25 mM HEPES, 300 mM NaCl, 25 mM imidazole, 5% glycerol, pH 7.5). The cell suspension was incubated at 4^{o}C in the presence of Protease Inhibitor Cocktail (Sigma-Aldrich), DNAse I, RNAse, and lysozyme. All subsequent steps were performed at 4^{o}C. Cells were lysed by sonication and the resultant lysate was clarified by centrifugation (34,500 *g* for 45 min). The clarified lysate was loaded onto three-in-tandem 5 mL HisTrap columns (GE Healthcare) equilibrated with buffer A. The column was washed with buffer A and *Af* SidA was eluted with a 200 mL imidazole gradient (25 – 300 mM) at a flow rate of 5 mL/min. Fractions containing His_8-MBP-SidA (as judged by SDS-PAGE) were pooled, then diluted with buffer A and concentrated to a 50 mL volume using an Amicon stirred cell concentrator (Billerica, MA). *Af* SidA was liberated from the His_8-MBP tag by the addition of tobacco etch virus (TEV) protease. After overnight cleavage, the protein solution was subjected to centrifugation (34,500 *g* for 15 min) to remove traces of precipitate. The resulting sample was loaded onto two-in-tandem 5 mL HisTrap columns equilibrated with buffer A. The liberated *Af* SidA was pooled and

concentrated to a 2 mL volume using a stirred cell concentrator. After removal of traces of precipitate by centrifugation, the sample was loaded onto a Superdex S-200 column (GE Healthcare) equilibrated with buffer C (25 mM HEPES, 125 mM NaCl, 5% glycerol, pH 7.5) and eluted at a flow rate of 2 mL/min. Fractions containing *Af* SidA (as judged by SDS-PAGE) were pooled, then diluted with buffer D (25 mM HEPES, 5% glycerol, pH 7.5) and loaded onto two-in-tandem DEAE columns (GE Healthcare) equilibrated with buffer D. *Af* SidA was eluted with a 200 mL gradient NaCl gradient (10 – 400 mM) at a flow rate of 5 mL/min. As the last step, fractions containing *Af* SidA were pooled and concentrated to a 1 mL volume. *Af* SidA concentration was measured using a calculated extinction coefficient (ε_{450} = 13,700 M^{-1} cm^{-1}). Aliquots were frozen in liquid nitrogen prior to storage at -80^{o}C.

2.2.4 Gel filtration chromatography

Af SidA (9.3 mg/mL) was loaded onto a Superdex S-75 column (GE Healthcare) equilibrated with buffer A and a final TCEP concentration of 300 µM. Aprotinin (6,500 Da), Ribonuclease A (13,700 Da), Ovalbumin (43,000 Da), Conalbumin (75,000 Da), Aldolase (158,000 Da) and Ferritin (440,000 Da) were used to determine the oligomeric state of the *Af* SidA species in solution.

2.2.5 Mass spectrometry

For mass spectral analysis of *Af* SidA, a portion of the protein was desalted using an OMIX C18 tip (Varian, Inc., Lake Forest, CA) following the manufacturer's directions. Then, the protein (approximately 125 µM) was mixed 1:1with 10 mg mL^{-1}

sinapinic acid (Aldrich) in 30:70 HPLC-grade acetonitrile/HPLC-grade water supplemented with 0.1% trifluoroacetic acid. A 1 µL aliquot was spotted onto a MALDI target plate and allowed to air-dry. The deposited sample was then analyzed in the linear positive ion-operating mode using an ABI 4800 MALDI TOF/TOF after calibration.

III. Results

Recombinant *Af* SidA was expressed as a fusion to maltose binding protein (MBP) in *E. coli* BL21T1^{R} cells. Soluble *Af* SidA was purified from cells induced for 4 hours by a series of chromatographic steps with a yield of 15 mg of highly active enzyme per 1 L of culture (Table 2.1). Induction time was important, as cells grown for more than 12 hours after induction expressed *Af* SidA as insoluble protein (data not shown). Moreover, expression of *Af* SidA in the absence of MBP yielded similar results. The subunit molecular mass of purified *Af* SidA, as determined by SDS-PAGE, was ~55 kDa (Figure 2.2). Furthermore, a molecular weight of 57,210 Da was determined by mass spectrometry analysis (Table 2.2). This is in agreement with the predicted molecular mass of 57,231 Da, based on the amino acid sequence. By gel filtration, the estimated native molecular mass of *Af* SidA was 228 kDa, suggesting that the enzyme adopts a tetrameric quaternary structure (Figure 2.3 and Table 2.2).

Table 2.1. Results of the expression and purification of *Af* SidA.

Vector	Expressed protein [a]	Expression Medium	Cell yield (g) [b]	Purified protein yield (mg/L)	Cofactor incorporation [c]
pVP55A	His8-*Af* SidA	LB – IPTG	22	0	No, insoluble
pVP56K	His8-MBP-*Af* SidA	LB – IPTG	25	15.0	Yes, ~ 60 %

[a] Schematic representations of the expression vectors are shown in Figure 2.1.

[b] Wet cell weight obtained per 9 liters of culture medium after centrifugation described in Materials and Methods.

[c] FAD content in His8-*Af* SidA or His8-MBP-*Af* SidA.

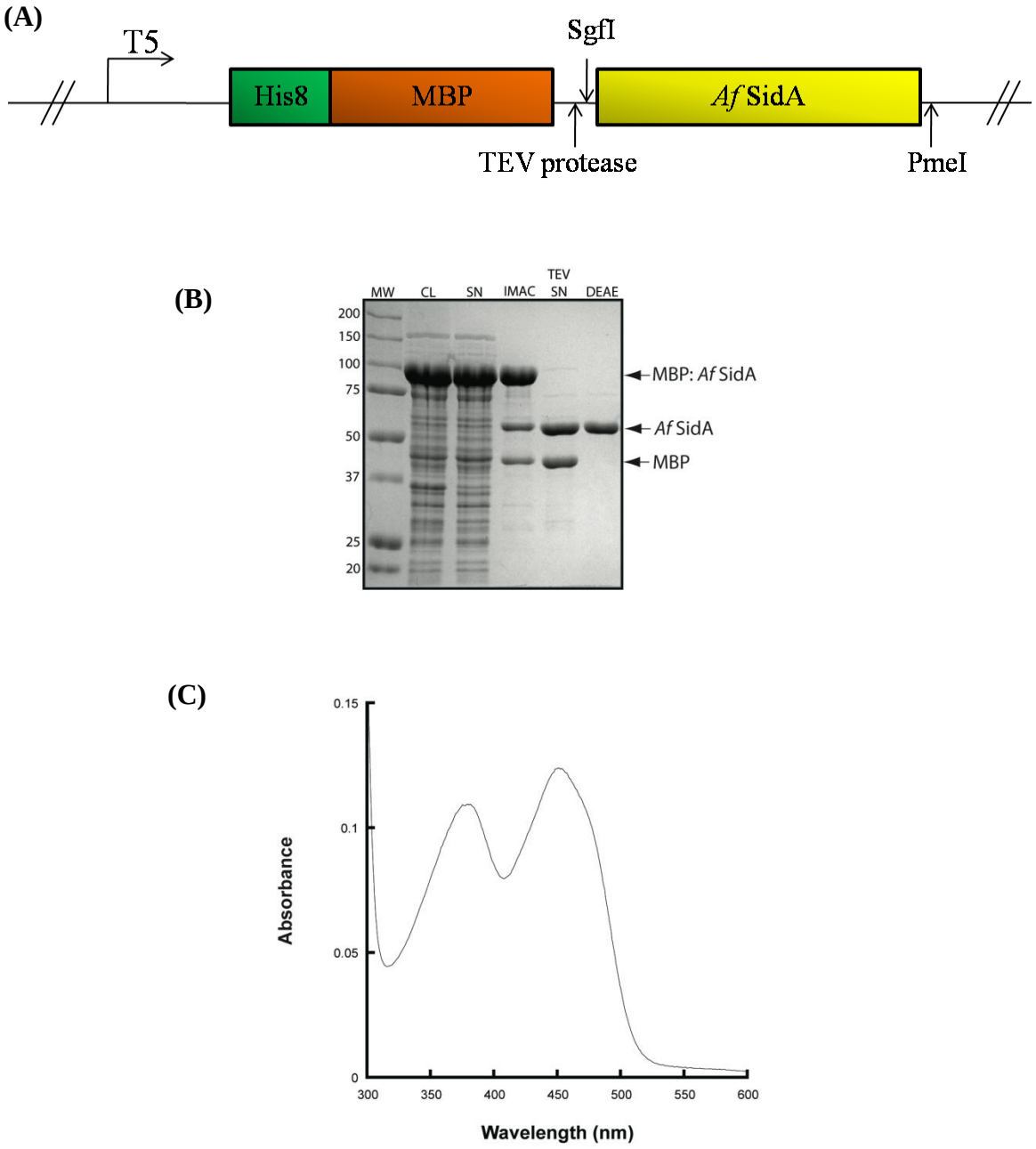

Figure 2.1. Summary of *Af* SidA purification. **(A)** Schematic of the pVP56K vector. **(B)** SDS-PAGE gel summarizing the purification of *Af* SidA. **(C)** UV-Visible spectrophotometry of bound FAD in purified *Af* SidA.

(A)

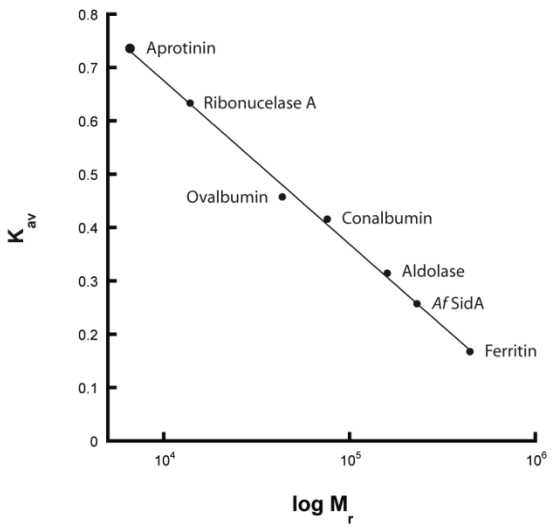

(B)

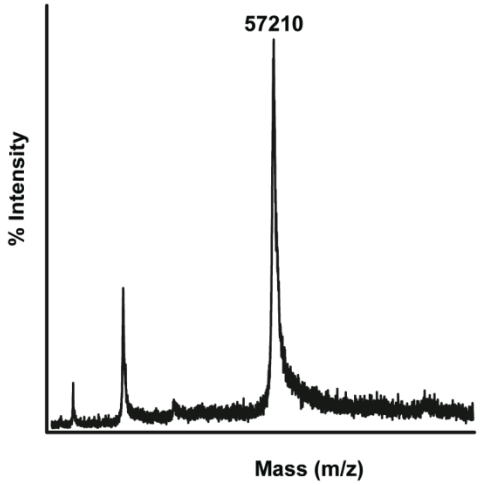

Figure 2.2. Solution molecular weight and mass spectrometry studies of *Af* SidA. **(A)** Standard curve generated to determine the molecular weight of *Af* SidA in solution. **(B)** Mass spectrometry analysis.

Table 2.2. Solution molecular weight and mass spectrometry studies of *Af* SidA.

Sample	**Technique**	**Predicted MW (Da)**	**Observed MW (Da)**
Af SidA	MALDI-TOF MS	57231	57210
Af SidA	SDS-PAGE	57231	55000
Af SidA (soln.)	Gel Filtration	232064	228000
FAD	MALDI-TOF MS	785.55	786

IV. Discussion

2.4.1Cloning *Af sidA*

The *Af sidA* gene contains one intron and cDNA was not available. Therefore, a codon-optimized sequence of *Af sidA* for expression in *E. coli* was obtained, thus preventing additional biological safety requirements. The *A. fumigatus sidA* gene was ligated into two plasmids using the Flexi® cloning system. Use of this versatile technique greatly reduced errors during the cloning experiments and allowed for other ligations using the same digested vectors. Results from this cloning strategy revealed that the *Af sidA* gene encoded a 57.2 kDa protein, which was slightly larger when compared to other NMOs, including PvdA (51.6 kDa), CchB (51.3 kDa), and VbsO (50.6 kDa).

2.4.2 *Af* SidA protein production and yield

Obtaining recombinant, soluble and active NMOs was a difficult task. In fact, work by the author has shown that even in the presence of fusion proteins and molecular chaperones, the NMOs from *M. tuberculosis* and *Y. pestis* remained in the insoluble fraction upon cell lysis (data not shown). Table 2.1 provides the results of the expression and purification of *Af* SidA. From this table, it is shown that *E. coli* cells yielding the soluble *Af* SidA were grown exclusively in LB media. Other attempts to obtain soluble and active forms of *Af* SidA were utilized, including the auto-induction method [61]. Although this technique provided approximately 65 g of wet cell paste, *Af* SidA was expressed as an insoluble protein. This could be a result of the expression time, which totaled over 12 hours. However, use of LB-IPTG expression medium resulted in a significant amount of soluble and highly active *Af* SidA.

2.4.3 Purification of *Af* SidA

The purification of *Af* SidA followed a logical pattern, although there were several issues that required special attention. First, *Af* SidA was expressed as a fusion to His_8-MBP (Figure 2.2). Therefore, the chromatographic logic was to first pass the whole-cell supernatant over a HisTrap column, which selectively binds proteins containing the histidine affinity tag. Cleavage and separation of *Af* SidA from MBP were next, followed by removal of any trace contaminants from *Af* SidA. These steps were chosen based upon affinity, charge, and size differences between *Af* SidA and the various contaminants. Second, this series of chromatographic steps did result in a soluble protein, although the process required several modifications. For example, *Af* SidA required a minimum NaCl concentration of 125 mM NaCl for optimal stability. Furthermore, the addition of 5% glycerol to each of the purification buffers increased the total protein yield by approximately 25%. Finally, by decreasing the flow rate of the ÄKTA Prime FPLC system, the total yield of *Af* SidA increased due to a lower pressure exerted on the protein. It is therefore apparent from the purification that *Af* SidA is sensitive to salt and glycerol concentrations, as well as the general hydrodynamic force exerted on the protein.

There are several key findings to note upon the purification of *Af* SidA. First, the optical spectrum in Figure 2.2 indicates the presence of an FAD cofactor bound to the purified enzyme. As a result, the extinction coefficient for the FAD cofactor was determined to be ε_{450} = 13,700 M^{-1} $cm^{-}1$. This is the first report of a member of the microbial NMOs containing high incorporation of FAD upon purification. VbsO was purified with bound FAD, although the cofactor incorporation was estimated at less than

5% [34]. Based upon the results from the primary amino acid sequence alignment, there do not appear to be significant differences among the putative FAD and NADPH binding domains (Figure 2.4). Nonetheless, the strong binding of FAD to *Af* SidA will permit extensive kinetic and structural analyses. Second, to obtain soluble *Af* SidA, the enzyme was expressed as a fusion to His_8-MBP. In contrast, other family members, including CchB and PvdA, were expressed and purified with only an N-terminal hexahistidine tag [58-60]. One possible explanation for this could be a markedly different hydrophobicity pattern of *Af* SidA.

2.4.4 Gel filtration

Gel filtration analyses revealed that *Af* SidA adopted a tetrameric quaternary structure (Figure 2.3). In conflicting reports, Ge and co-workers originally reported PvdA as adopting either a tetrameric or pentameric quaternary structure upon gel filtration analysis [59]. These results, however, were contradicted by Meneely and co-workers who revealed through dynamic light scattering that PvdA likely existed as a monomer [58]. With respect to the functionally related L-lysine N^6-oxygenase, IucD, Plattner and co-workers determined that purified IucD existed as a tetramer [62]. From these studies, the quaternary structure among NMOs appears to vary among species.

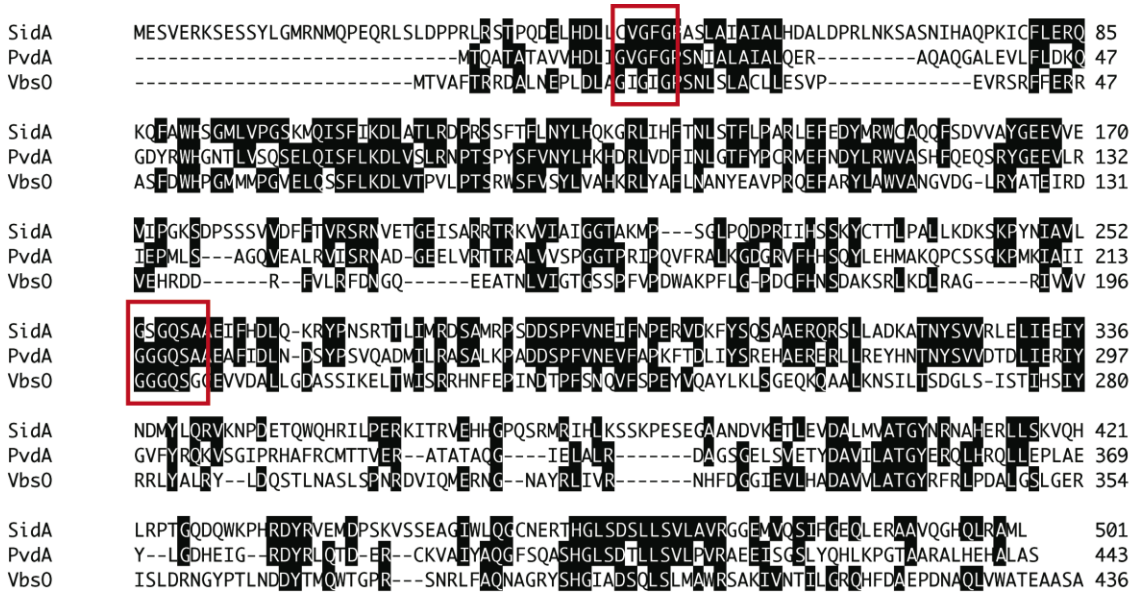

Figure 2.3. Multiple amino acid sequence alignment of L-ornithine N^5-oxygenases. Sequences presented above include those from *Aspergillus fumigatus* (*Af* SidA), *Pseudomonas aeruginosa* (PvdA) and *Rhizobium etli* CFN42 (VbsO). Conserved residues are shaded in black. Highlighted areas indicate two Rossmann folds for FAD and NADPH binding.

CHAPTER THREE

Steady-State Kinetic Characterization of *Af* SidA

I. Introduction

Af SidA is a member of the Class B flavoprotein monooxygenases (E.C. 3.2.3) [63]. General characteristics of this subclass include flavoproteins that: (*i*) are encoded by a single gene, (*ii*) contain a tightly bound FAD cofactor, (*iii*) depend on NADPH for reducing equivalents, (*iv*) keep the coenzyme NADPH/$NADP^+$ bound during catalysis and are (*v*) composed of two dinucleotide binding domains binding FAD and NADPH [63]. This subclass is also referred to as mixed-function flavoprotein monooxygenases as representatives of this subclass are able to oxidize a variety of nucleophilic and electrophilic substrates. This subclass comprises three-sequence related flavoprotein monooxygenases: (*i*) flavin-containing monooxygenases (FMOs), (*ii*) microbial N-hydroxylating monooxygenases (NMOs) and (*iii*) Baeyer-Villiger monooxygenases (BVMOs) [64]. The catalytic cycle of flavoprotein monooxygenases can be divided into two half-reactions. In the reductive half-reaction, oxidized flavin (Figure 3.1, I) is reduced via a hydride transfer from NADPH. The reduced flavin (II) will then proceed to react with molecular oxygen to form a C4a-(hydro)peroxyflavin intermediate (III), at which point the substrate will react with the distal oxygen of the flavin, resulting in hydroxylated product and a hydroxyflavin (IV). From here, the hydroxyflavin dehydrates to reform the oxidized FAD. These latter steps are collectively referred to as the oxidative half-reaction. In this chapter, the steady-state kinetic parameters of *Af* SidA are presented, while differences between substrate preferences and kinetic mechanisms among the flavin-containing monooxygenases are also discussed.

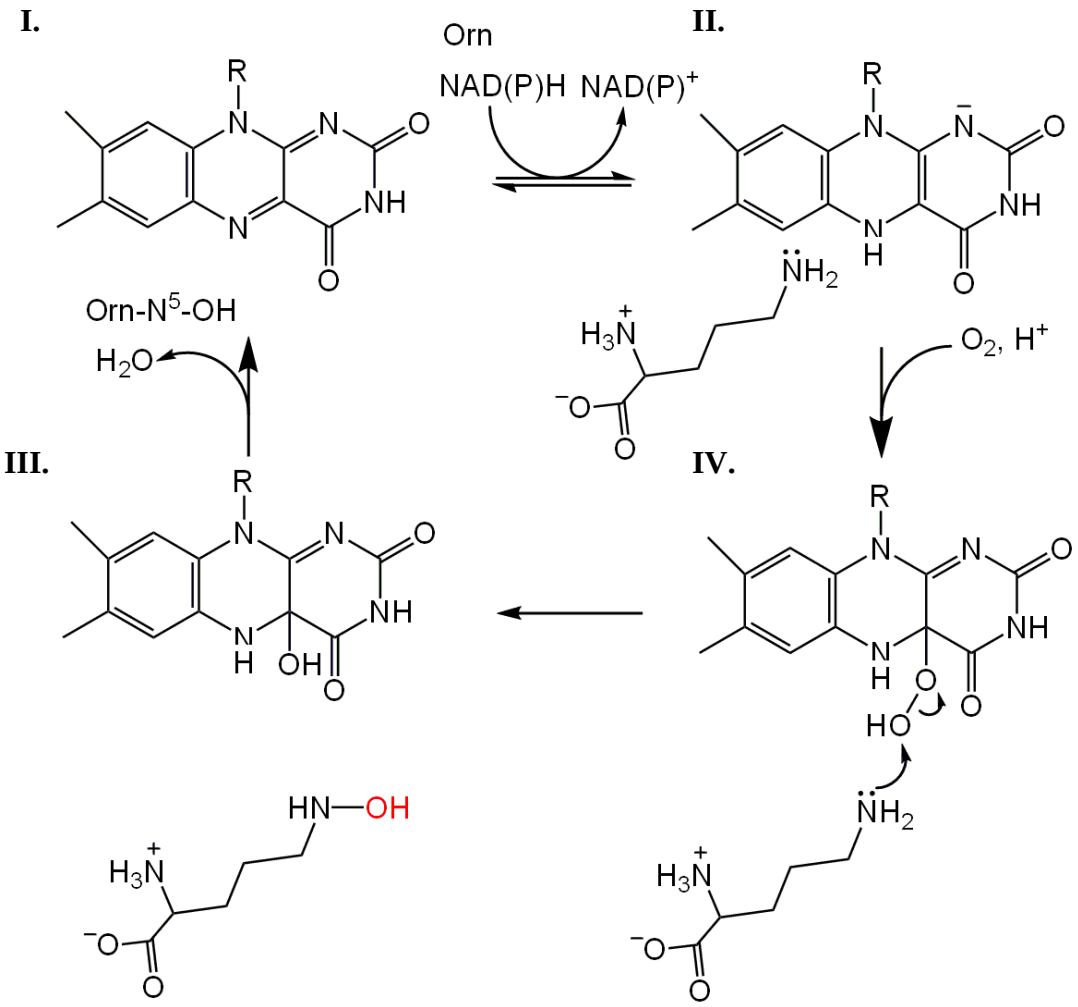

Figure 3.1. Proposed reaction mechanism for *Af* SidA.

II. Materials and Methods

3.2.1 Product formation assay

The amount of hydroxylated product formed by *Af* SidA was assayed by a variation of the Csaky iodine oxidation reaction [62, 65]. The standard assay buffer contained 100 mM phosphate, pH 7.5 and L-ornithine. *Af* SidA (2.0 μM) was incubated in 92 μL of assay buffer at 25°C before the reaction was initiated by the addition of 1 mM NADPH. The reaction proceeded for 10 min at 25°C with shaking, at which time the assay mixture was withdrawn and added to 52.5 μL of 0.2N perchloric acid to terminate the reaction. For each L-ornithine concentration, 62.5 μL of the terminated reaction mixture was transferred into a 0.5 mL microcentrifuge tube and the reaction mixture was neutralized by the addition of 62.5 μL of 5% (w/v) sodium acetate solution. To each tube were added 62.5 μL of 1% (w/v) sulfanilic acid in 25% (v/v) acetic acid and 25 μL of 1.3% (w/v) potassium iodide in glacial acetic acid and the reaction was incubated with shaking at 25°C for 7 min. Excess iodine was removed with 25 μL of 0.1 N sodium thiosulfate and the color was developed by adding 25 μL of 0.6% (w/v) α-naphthylamine in 30% (v/v) acetic acid. The absorbance at 562 nm was measured after 15 min on a SpectraMax M5e plate reader (Molecular Devices). A standard curve of hydroxylamine hydrochloride was used to calculate the amount of hydroxylated product produced.

3.2.2 Oxygen consumption assay

The amount of molecular oxygen consumed by *Af* SidA was monitored using a Hansatech Oxygraph (Piscataway, NJ). The standard assay buffer consisted of 100 mM phosphate, pH 7.5 and L-ornithine. *Af* SidA (2.0 μM) was incubated in 439 μL of assay

buffer at 25^{o}C before the reaction was initiated by the addition of 1 mM NADPH. The reaction proceeded for one min at 25^{o}C, with constant stirring, at which time measurements of the slope (nmol min^{-1} mL^{-1} of oxygen consumed) were taken directly from the program.

3.2.3 Determination of enzyme specificity and kinetic parameters

A variety of modifications of the standard assay conditions were tested. An ionic strength of 0.1 M with 5% glycerol promoted protein solubility and stability and was used for storage of *Af* SidA. Both the product formation and oxygen consumption assays were used to determine enzyme specificity. For the coenzyme substitution reactions, NADPH was replaced by NADH at comparable concentrations. For the substrate substitution reactions, 15 mM L-ornithine was substituted with 15 mM L-lysine, L-arginine, L-cysteine, L-serine, L-norvaline, histamine or tryptamine. The kinetics of *Af* SidA were assayed similarly, by varying the L-ornithine concentrations from 0 to 15 mM and NADPH from 0 to 6 mM.

3.2.4 Hydrogen peroxide formation assay

The procedure described by Hildebrandt and co-workers was used [66]. The standard assay buffer is the same as described for the hydroxylation assay. The amount of hydrogen peroxide formed was determined in conjunction with the amount of hydroxylated product formed. The reaction was initiated by the addition of 1 mM NAD(P)H to *Af* SidA (2.0 µM) incubated in the assay buffer at 25^{o}C. After the initial 9 min reaction, the remaining 104 µL, the reaction was terminated by the addition of an

equal volume of 3% (w/v) trichloroacetic acid. The terminated reaction was clarified by centrifugation (2,600 *g* for 5 min). The resulting supernatant was transferred to a clean 0.5 mL microcentrifuge tube and treated with 82 μL of 10 mM ferrous ammonium sulfate, followed by 26 μL of 2.5 M potassium thiocyanate. The mixture was incubated for 10 min at 25^{o}C with shaking, at which time the absorbance at 480 nm was recorded. A standard curve of hydrogen peroxide was used to calculate the amount of hydrogen peroxide produced by *Af* SidA.

3.2.5 Detection of the C4a-(hydro)peroxyflavin

In studies of the reactions of *Af* SidA with reduced coenzymes, buffer (100 mM phosphate, pH 7.5) and $NADP^+$ (33 μM) were mixed and scanned on an Agilent 8453 spectrophotometer (Santa Clara, CA). This mixture served as the blank. *Af* SidA (11 μM) was then added to the solution and a spectrum of the oxidized enzyme was recorded. The reaction was then initiated by the addition of NADPH (22 μM). Using the kinetics mode on the software, the instrument was programmed to record a separate spectrum every 0.5 sec for five minutes in the range of 200 – 1100nm. Other ratios of $NADP^+$: *Af* SidA : NADPH were tested, however, concentrations of NADPH greater than 3-fold more than the concentration of *Af* SidA resulted in the interference of absorbance by the reduced coenzyme in the 320 – 350 nm range.

3.2.6 Data analysis

Kinetic data were analyzed using the programs KaleidaGraph (Adelbeck Software, Reading, PA) and EnzFitter (BioSoft, Cambridge, UK). Initial rata data were fit to the Michaelis-Menten equation to obtain k_{cat} and K_m values in eq. 1. Eq. 2 describes the effects of substrate inhibition during reduced coenzyme saturation curves. Eq. 3 describes competitive inhibition by $NADP^+$, whereas eq. 4 describes uncompetitive inhibition by chloride. Halide inhibition curves were fit to eq. 5, which describes the concentration of inhibitor at 50% activity; here y_{max} and y_{min} refer to the upper and lower reaction rate limits.

$$v = \frac{V\mathrm{max}\ [\mathrm{S}]}{K\mathrm{m}+[\mathrm{S}]} \qquad (1)$$

$$v = \frac{Vmax\ [S]}{Km+[S]+\left(\frac{[S]^2}{KI}\right)} \qquad (2)$$

$$v = \frac{V\mathrm{max}\ [\mathrm{S}]}{K\mathrm{m}\left[1+\frac{\mathrm{I}}{\mathrm{KI}}\right]+[\mathrm{S}]} \qquad (3)$$

$$v = \frac{V\mathrm{max}\ [\mathrm{S}]}{K\mathrm{m}\left[1+\frac{\mathrm{I}}{\mathrm{KII}}\right]+[\mathrm{S}]\left[1+\frac{\mathrm{I}}{\mathrm{KIS}}\right]} \qquad (4)$$

$$v = \frac{y\mathrm{min}+(y\mathrm{max}-y\mathrm{min})}{[1+\left(\frac{\mathrm{X}}{\mathrm{IC}\,50}\right)^{\mathrm{m}}]} \qquad (5)$$

III. Results

3.3.1 Steady-state kinetics with substrate

The steady-state kinetic parameters of *Af* SidA using the product formation and oxygen consumption assays are presented in Table 3.1. With NADPH as the electron donor, *Af* SidA exclusively hydroxylated L-ornithine with an apparent k_{cat} of 29 ± 0.3 min^{-1} using the product formation assay and an apparent k_{cat} of 41 ± 0.8 min^{-1} using the oxygen consumption assay. Unexpectedly, with NADH as the electron donor, *Af* SidA also hydroxylated L-ornithine with an apparent k_{cat} of 31 ± 0.8 min^{-1} using the product formation assay and an apparent k_{cat} of 52 ± 1.0 min^{-1} using the oxygen consumption assay. Using NADPH, the apparent binding affinity of L-ornithine was calculated to be 1.7 ± 0.1 mM with the product formation assay and 0.5 ± 0.1 mM with the oxygen consumption assay. Similarly, the apparent binding affinity of L-ornithine was calculated to be 1.7 ± 0.1 mM with the product formation assay and 2.0 ± 0.1 mM with the oxygen consumption assay using NADH as the electron donor (Figure 3.2).

3.3.2 Steady-state kinetics with coenzymes

The product formation and oxygen consumption assays provided the apparent binding affinity of NADPH as 940 ± 180 μM and 31 ± 2.0 μM, respectively. In experiments where NADPH was substituted by NADH, the apparent binding affinity was calculated to be 490 ± 224 μM using the product formation assay and 214 ± 12 μM using the oxygen consumption assay (Figure 3.3). Use of the oxygen consumption assay provided kinetic parameters for the inhibition of *Af* SidA by $NADP^+$. The resulting rates, plotted as double-reciprocal plots, provided an inhibition constant, K_I of 597 ± 18 μM

and indicated a pattern of competitive inhibition by $NADP^+$ since the lines were not parallel, but intersected at the *y*-intercept (Figure 3.4).

3.3.3 Oxygen activation by substrate and analogs

To further explore the reactivity of *Af* SidA, the rates of product formation and oxygen consumption of *Af* SidA were measured after the addition of L-ornithine, as well as a series of structurally related compounds. These results are presented in Table 3.2. Upon the addition of L-ornithine, the rate of oxygen consumption increased 27-fold over the rate in the absence of L-ornithine. Conversely, L-arginine, L-cysteine, histamine, L–norvaline, L-serine and tryptamine did not stimulate the rate of oxygen consumption and no hydroxylated product was formed. Interestingly, oxygen consumption was increased 17-fold upon the addition of L-lysine, although no hydroxylated product was formed.

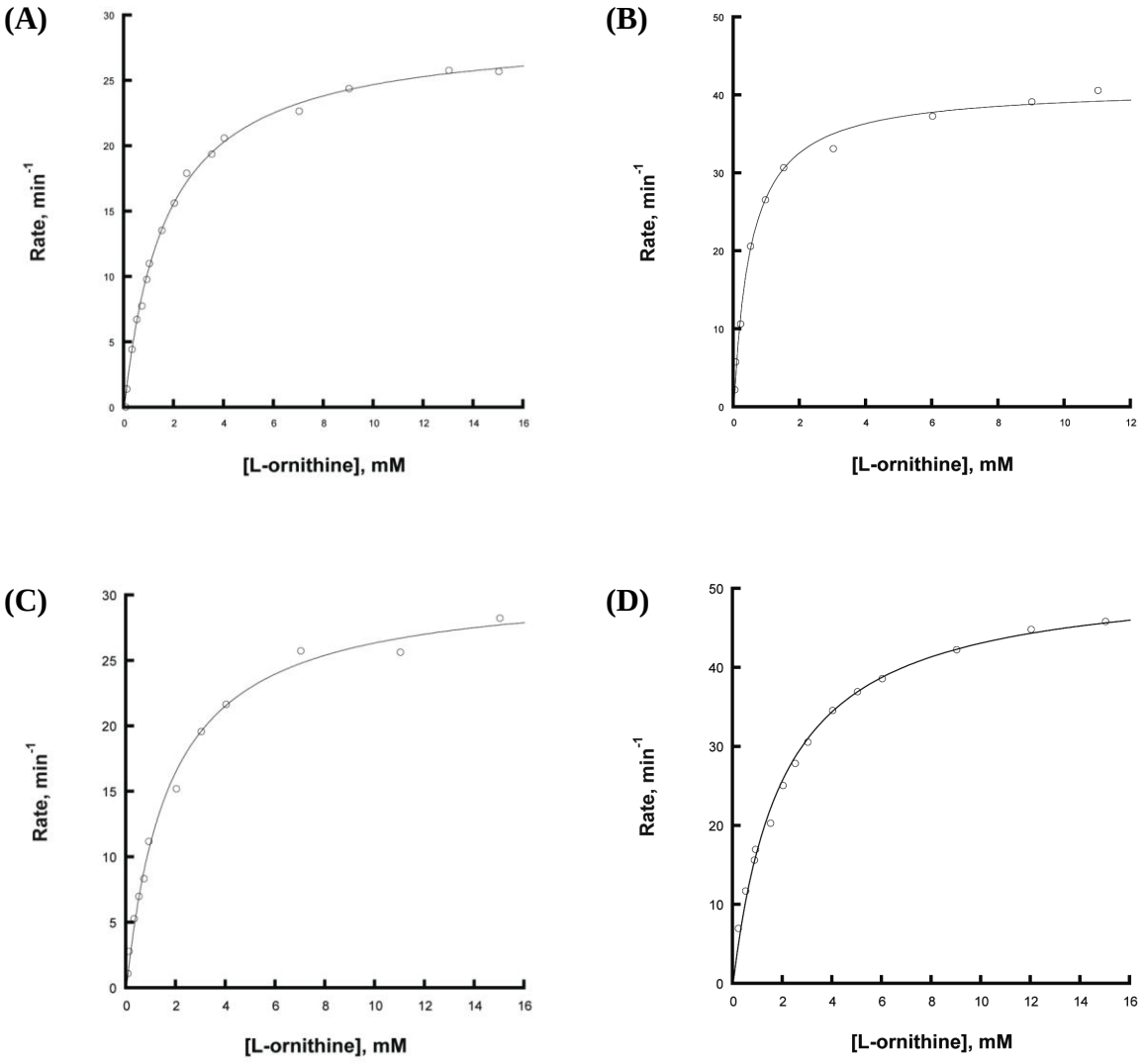

Figure 3.2. L-ornithine saturation kinetics of *Af* SidA as determined by the product formation and oxygen consumption assays. Substrate saturation curves using NADPH in the product formation **(A)** and oxygen consumption **(B)** assays. Substrate saturation curves using NADH in the product formation **(C)** and oxygen consumption **(D)** assays.

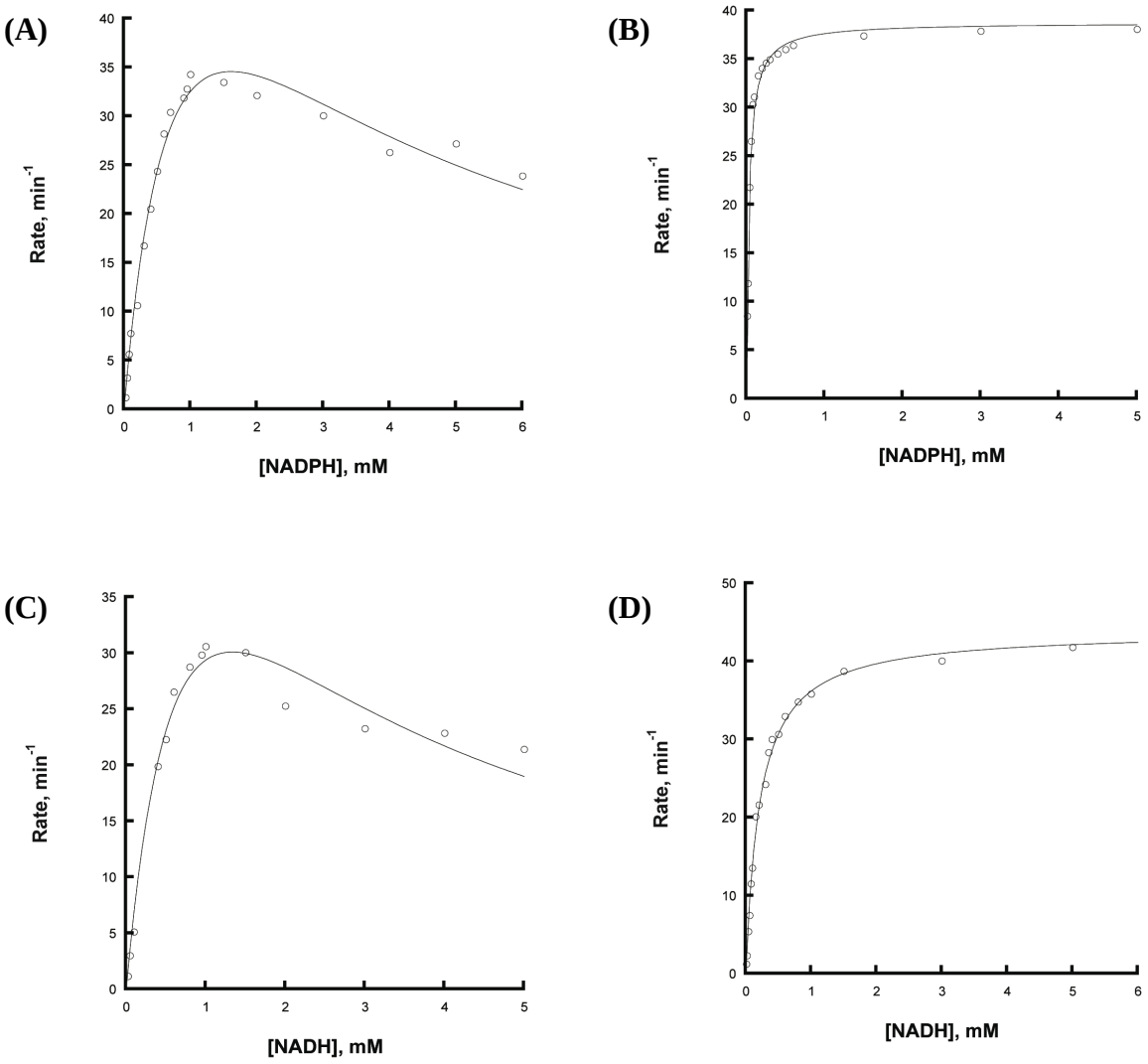

Figure 3.3. Reduced coenzyme saturation kinetics of *Af* SidA as determined by the product formation and oxygen consumption assays. Reduced coenzyme saturation curves using NADPH in the product formation **(A)** and oxygen consumption **(B)** assays. Reduced coenzyme saturation curves using NADH in the product formation **(C)** and oxygen consumption **(D)** assays.

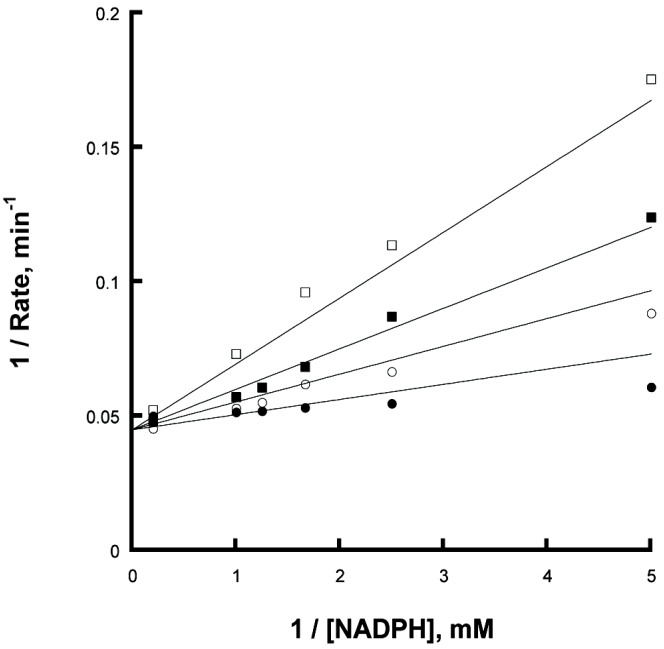

Figure 3.4. Inhibition of *Af* SidA by $NADP^+$ as determined by the oxygen consumption assay. Double reciprocal plots of rates as a function of NADPH concentration. $NADP^+$ concentrations used were (●) 0 mM, (○), 500 μM, (■)1 mM, and (□) 2 mM.

Table 3.1. Summary of *Af* SidA kinetic parameters.

Product Formation Assay			
Parameter	NADPH	NADH	Equation
k_{cat} (min^{-1})	29 ± 0.3	31 ± 0.8	1 [a]
$K_{m,\ L\text{-}orn}$ (mM)	1.7 ± 0.1	1.7 ± 0.1	1 [a]
k_{cat} / $K_{m,\ L\text{-}orn}$ (min^{-1} mM^{-1})	17 ± 0.4	18 ± 1.1	1 [a]
$K_{m,\ coenzyme}$ (μM)	940 ± 180	490 ± 224	2 [a]
$K_{I,\ coenzyme}$ (mM)	2.8 ± 0.6	2.1 ± 0.9	2 [a]

Oxygen Consumption Assay			
Parameter	NADPH	NADH	Equation
k_{cat} (min^{-1})	41 ± 0.8	52 ± 1.0	1 [a]
$K_{m,\ L\text{-}orn}$ (mM)	0.5 ± 0.1	2.0 ± 0.1	1 [a]
k_{cat} / $K_{m,\ L\text{-}orn}$ (min^{-1} mM^{-1})	80 ± 6	26 ± 1.1	1 [a]
$K_{m,\ coenzyme}$ (μM)	31 ± 2	214 ± 12	1 [a]
k_{cat} / $K_{m,\ coenzyme}$ (min^{-1} mM^{-1})	1263 ± 89	205 ± 9	1 [a]
$K_{I,\ NADP+}$ (μM)	597 ± 18		3 [a]

[a] Equations are provided in Materials and Methods of this chapter.

Table 3.2. Summary of *Af* SidA coenzyme and substrate specificities.

Test conditions	Product formation assay (Rate, min^{-1})	Oxygen consumption assay (Rate, min^{-1})
	Omission test	
no omission	29 ± 0.3	41 ± 0.8
- *Af* SidA		1.1 ± 0.1
- L-ornithine		1.5 ± 0.1
	Specificity	
- NADPH		
+ NADH	31 ± 0.8	52 ± 1.0
- L-ornithine		
+ L-arginine	*a*	*a*
+ L-cysteine	*a*	*a*
+ Histamine	*a*	*a*
+ L-lysine	*a*	26 ± 3.5
+ L-norvaline	*a*	*a*
+ L-serine	*a*	*a*
+ Tryptamine	*a*	*a*

[a] Below the limits of detection (< 2 min^{-1}).

3.3.4 Oxygen activation versus substrate hydroxylation

Not every molecule of O_2 consumed by *Af* SidA was channeled toward product formation. To account for oxygen consumption channeled towards non-productive turnover, Figure 3.5 illustrates the production of hydrogen peroxide, both as a function of L-ornithine and reduced coenzyme. Here, it was seen that hydrogen peroxide formation decreased as a function of L-ornithine concentration in the presence of both coenzymes, ranging from 50 to 25 μmol produced with NADPH as the reduced coenzyme and 195 to 45 μmol produced with NADH as the reduced coenzyme. The amount of hydrogen peroxide also increased as a function of each coenzyme, ranging from 5 to 60 μmol produced with NADPH as the reduced coenzyme and 12 to 135 μmol produced with NADH as the reduced coenzyme.

3.3.5 Oxygenated flavin intermediates

By use of excess amounts of NADPH (two-fold) and $NADP^+$ (three-fold), aerobic reduction of *Af* SidA was monitored as a decrease in absorbance at 450 nm. Although a rate constant was not determined, a stable C4a-(hydro)peroxyflavin intermediate was detected (Figure 3.6). This flavin intermediate was determined to have a half-life of 28.8 seconds. In separate experiments, NADPH was substituted with NADH and no stable peroxyflavin was detected.

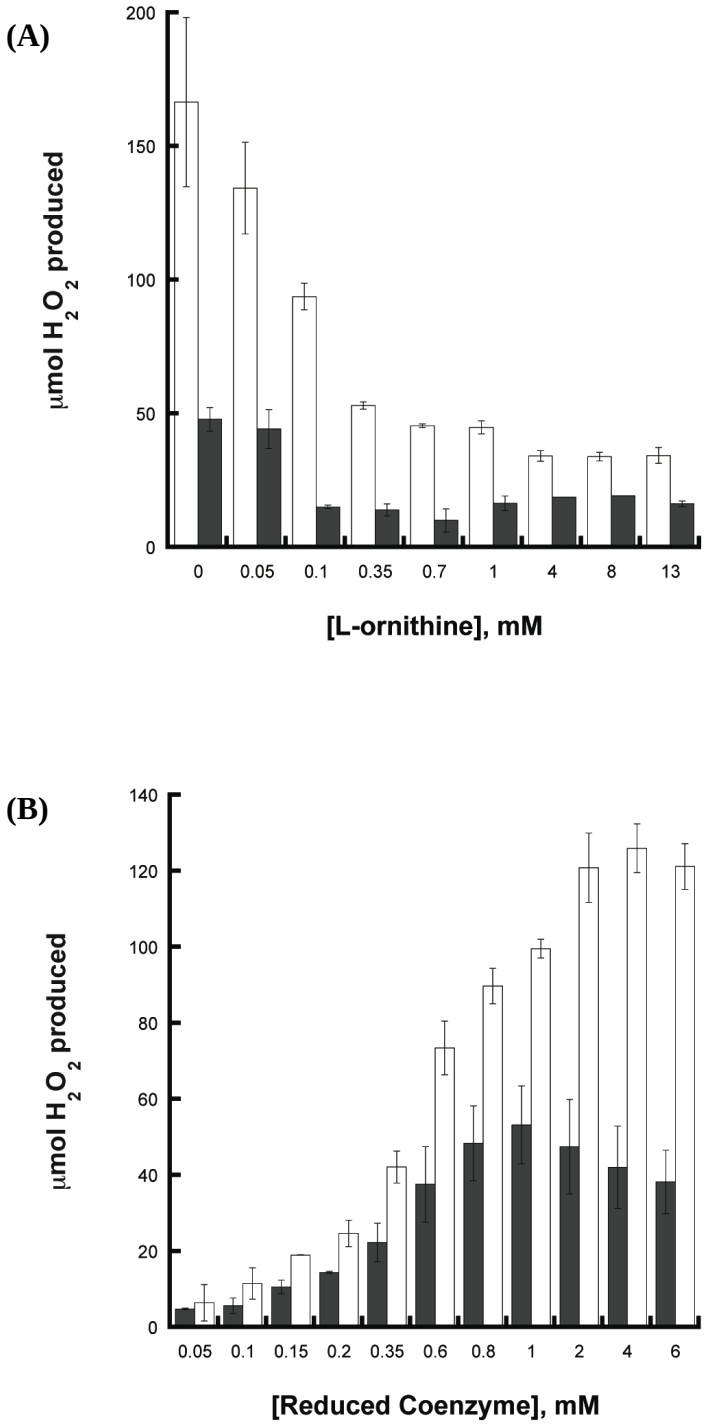

Figure 3.5. H_2O_2 production by *Af* SidA as a function of L-ornithine and reduced coenzyme. The amounts of H_2O_2 produced were measured for NADPH (solid bars) and NADH(open bars).

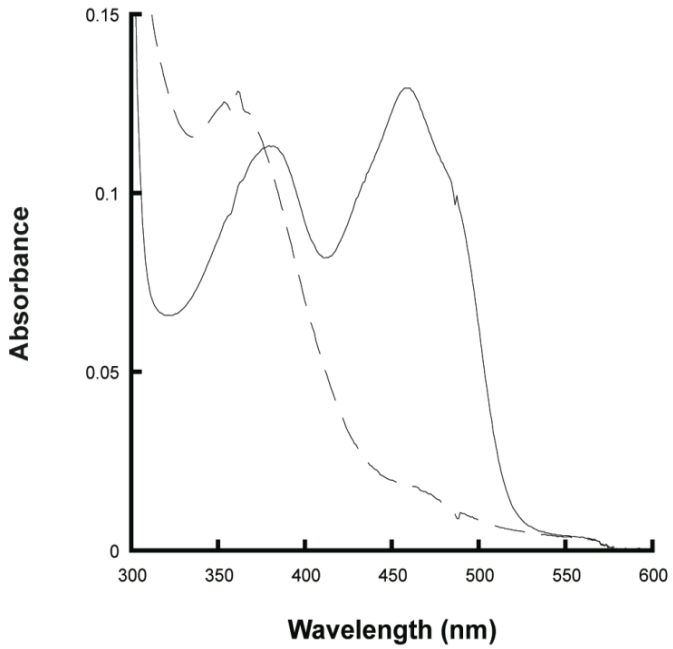

Figure 3.6. Detection of a stable C4a-flavin peroxide by *Af* SidA. Upon addition of two-fold excess NADPH to oxidized *Af* SidA, UV-Visible traces indicate the rapid formation of a stable (hydro)peroxyflavin intermediate necessary for catalysis.

IV. Discussion

3.4.1 Steady-state kinetics with substrate

The Michaelis-Menten kinetic parameters of *Af* SidA for L-ornithine hydroxylation were determined to be an apparent k_{cat} of 29 ± 0.3 min^{-1} using NADPH and an apparent k_{cat} of 31 ± 0.8 min^{-1} using NADH as determined by the product formation assay. These kinetic parameters are comparable with those reported for PvdA and the functionally related L-lysine N^6-oxygenase, IucD [67]. In contrast, the values obtained for *Af* SidA are approximately two-fold higher than those reported for CchB [60]. On the other hand, VbsO appeared to exhibit the highest catalytic rate, with an apparent k_{cat} value five-fold higher than those reported for *Af* SidA and PvdA [34]. For comparison, the apparent binding affinity of *Af* SidA for L-ornithine (1.7 ± 0.1 mM) was approximately three-fold higher than the reported K_m value for PvdA as determined by the product formation assay [58]. The K_m values for other NMOs could not be directly compared to *Af* SidA since the rates were recorded using an NADPH oxidation assay.

As predicted for NMOs, *Af* SidA was highly specific for its substrate, L-ornithine (Table 3.2). Modifications that included shortened carbon-chain lengths, replacement of the terminal amine group, or the introduction of aromatic groups linked to amines, did not stimulate oxygen consumption in *Af* SidA, nor was hydroxylated product formed. Only L-lysine stimulated oxygen consumption, but substrate hydroxylation did not occur. To this end, the data suggest that L-lysine may act as a non-substrate effector, but *Af* SidA requires L-ornithine correctly positioned in close proximity to the C(4a) position of the isoalloxazine ring of the FAD cofactor to stimulate turnover.

3.4.2 Steady-state kinetics with coenzymes

With respect to the reduced coenzyme saturation curves, *Af* SidA suffered from inhibition of activity using the product formation assay, promoting uncoupling of the reaction and formation of hydrogen peroxide (Figure 3.5). In contrast, excess coenzyme concentrations did not inhibit *Af* SidA using the oxygen consumption assay. This pattern of inhibition with respect to coenzyme is not reported with other L-ornithine N^5-oxygenases, although substrate inhibition was reported as a function of L-ornithine (PvdA) or L-lysine (IucD). Figure 3.7 depicts that molecular oxygen only binds to the reduced form of the enzyme, but does not dictate the fate of the C4a-(hydro)peroxyflavin intermediate or product formation. As a result, oxygen consumed by *Af* SidA has two possible outcomes: (*i*) productive turnover where L-ornithine abstracts one oxygen atom from the flavin C4a-position for substrate hydroxylation and the second oxygen atom is released as water or (*ii*) the FAD cofactor undergoes non-productive turnover where both oxygen atoms are released as hydrogen peroxide. Therefore, patterns of inhibition were not observed using the oxygen consumption assay since it is measured different chemical steps in the reaction than did the product formation assay, resulting in differing rates.

Results from the coenzyme saturation kinetics may suggest that release of the oxidized coenzyme is the ultimate catalytic step, since $NADP^+$ was shown to be a competitive inhibitor of *Af* SidA (Figure 3.4). Thus, it is likely that the decrease in activity resulted from $NADP^+$ and NADPH competing for the same binding site on *Af* SidA. Consistent with the kinetic mechanism of the Baeyer-Villiger monooxygenase, phenylacetone monooxygenase (PAMO), release of $NADP^+$ is the rate-limiting step and likely controls the amount of hydroxylated product formed.

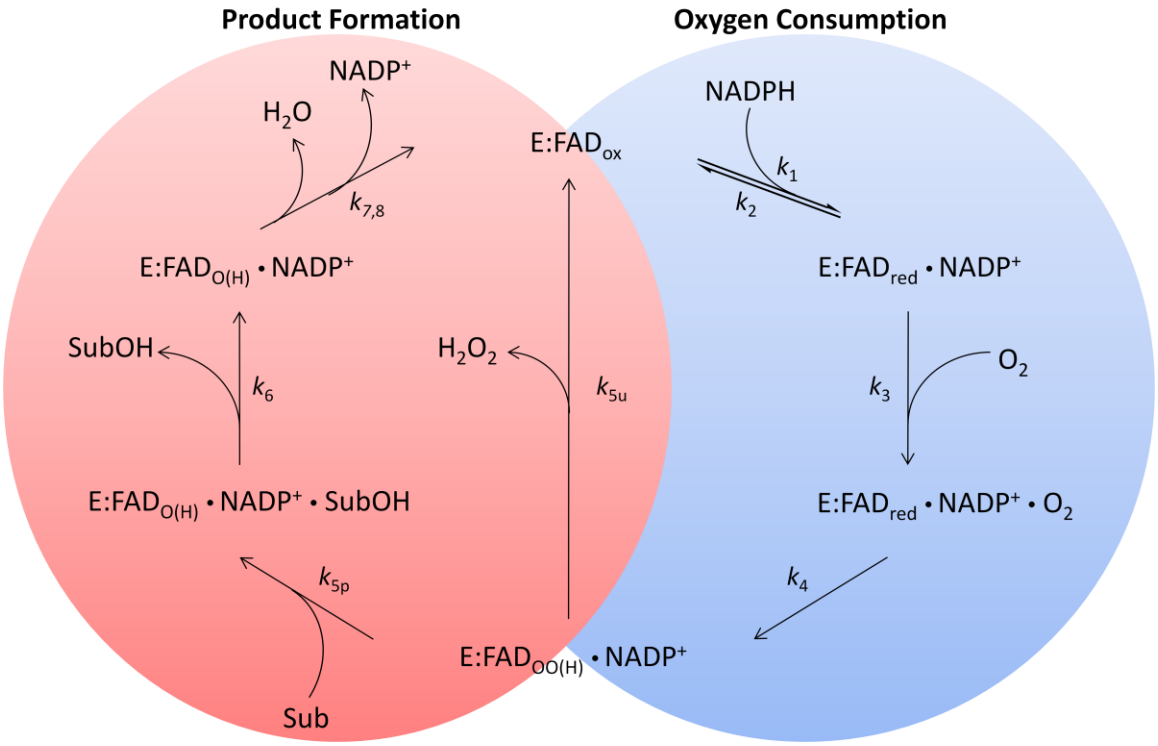

Figure 3.7. Reaction schemes of *Af* SidA with molecular oxygen.

3.4.3 Coenzyme promiscuity

Perhaps the most intriguing observation concerning the steady-state kinetics of *Af* SidA was the promiscuity of *Af* SidA to accept reducing equivalents from both NADPH and NADH. Similar to *Af* SidA, mFMO (hog liver microsomes) and IucD also were reported to utilize both NADPH and NADH as reducing equivalents. In the case of IucD, Thariath and co-workers mentioned that NADPH was the preferred electron donor for flavin reduction and NADH was half as effective as NADPH [68]. In a similar manner, Jones and co-workers demonstrated that mFMO was reduced by both NADPH and NADH. Despite this, NADH could only stabilize the hydroperoxyflavin intermediate of the enzyme 17% as effective as NADPH [69].

However, *Af* SidA, IucD, and mFMO appear to be rare exceptions for this class of flavoprotein monooxygenases. In fact, in coenzyme oxidation experiments, PvdA and CchB observed no stimulated oxidation when NADPH was substituted by NADH [58, 60]. It should be noted with respect to PvdA, however, hydroxylated product was detected at 14% of full activity when NADH replaced NADPH as the electron donor. This may suggest the possibility of nonspecific product formation in the presence of NADH [58].

To resolve the issue of coenzyme preference, reduced coenzyme saturation curves were performed using the oxygen consumption assay. Figure 3.3 indicates that there were clear differences between the apparent binding affinities of NADPH and NADH toward *Af* SidA. With NADPH as the electron donor, a K_m value of 31 ± 2 μM was obtained, while a K_m value of 214 ± 12 μM was obtained with NADH, demonstrating a seven-fold decrease in the apparent binding affinity. Therefore, when NADH served as the electron

donor, higher amounts of molecular oxygen were channeled toward hydrogen peroxide formation (Figure 3.5). From these data, it is concluded that *Af* SidA prefers NADPH versus NADH based on a lower K_m for NADPH using the oxygen consumption assay, in addition to an increased coupling of oxygen consumption and substrate hydroxylation.

3.4.4 Assignment of a kinetic mechanism to *Af* SidA

Figure 3.8 provides schematics for the mechanism of substrate hydroxylation of several well-characterized flavin-containing monooxygenases. The inherent differences in the mechanism among the flavin-containing monooxygenases predominantly originate from the order of substrate addition and product release. Within the past few decades, the mechanisms for mFMO, PAMO, *p*-hydroxybenzoate hydroxylase (PHBH), and PvdA have each been well characterized [70-72]. The mechanism that PHBH uses for substrate hydroxylation is considerably different than mFMO, PAMO and PvdA. PHBH requires substrate to be bound to the enzyme for FAD reduction by NADPH, followed by the dissociation of $NADP^+$ from the enzyme and subsequent binding of molecular oxygen. The reduced flavin then reoxidizes, passing through two intermediate states before finally forming the oxidized flavin, hydroxylated product, and water [70].

On the other hand, mFMO, PAMO and PvdA do not require substrate to be bound for flavin reduction or for oxygen binding. Instead, the flavin is reduced by NADPH and then binds molecular oxygen to form a (hydro)peroxyflavin intermediate that reacts with an oxidizable substrate to form the hydroxylated product and water. The major distinction between mFMO and PvdA versus PAMO is the peroxyflavin intermediate

formed during the catalytic cycle. In the case of mFMO and PvdA, the protonated hydroperoxyflavin is formed, while in PAMO, the unprotonated anion is formed.

The data gathered in this study helps provide a mechanism for *Af* SidA . First, *Af* SidA could be reduced in the absence of L-ornithine, indicating that this substrate is not likely to bind to the oxidized form of the enzyme (Figure 3.6). In mFMO, PAMO and PvdA, flavin reduction is independent of substrate. In fact, the reduced flavin cofactor of mFMO reacts with molecular oxygen and forms a stable C4a-hydroperoxyflavin (half-life of 2 hr at pH 7.2, 4^{o}C) until substrate binds [73]. For comparison, reoxidation of FAD occurs within 100 sec in PvdA [72]. Second, the half-life of the C4a-(hydro)peroxyflavin of *Af* SidA is several orders of magnitude less than mFMO, but is comparable with those obtained from PAMO and PvdA. The fact that this intermediate species could be detected suggests that its rate of formation must be faster than its rate of decomposition and it is not likely to be the rate-limiting step. Furthermore, in the presence of L-ornithine, the rate of flavin reoxidation is significantly accelerated, indicating that binding of substrate stimulates flavin recycling (Table 3.2).

Third, Figure 3.4 illustrates the inhibition of *Af* SidA by $NADP^+$ using the oxygen consumption assay. It was determined from these data that $NADP^+$ was a competitive inhibitor as a function of NADPH concentration. This suggests that $NADP^+$ and NADPH compete for the same binding site on *Af* SidA, as well as the same oxidized form of the enzyme. This supports the hypothesis that NADPH is the first substrate to bind to *Af* SidA, thereby reducing the flavin. From here, the reduced flavin likely reacts with molecular oxygen, forming the C4a-(hydro)peroxyflavin intermediate. Next, it seems logical that L-ornithine triggers substrate hydroxylation and after which, $NADP^+$ is

released, completing turnover. These findings suggest that *Af* SidA follows a sequential-ordered mechanism most closely related PAMO and PvdA [71, 72, 74]. However, further studies are needed to answer the question of the exact order of substrate addition and product release. Such experiments include determining the rates of FAD reduction and reoxidation, as well as these rates in the presence or absence of substrate.

It should also be noted that during this discussion the exact flavin peroxide species formed by *Af* SidA was intentionally assigned as a "(hydro)peroxyflavin." This ambiguous notation is due to a lack of information on the exact protonation state of the C4a position of the isoalloxazine ring. It seems logical that during substrate hydroxylation L-ornithine would perform a nucleophilic attack on the protonated distal oxygen atom located at the C4a-locus. However, further experiments are needed to elucidate the correct flavin intermediate formed in the presence and absence of L-ornithine.

(A) PHBH

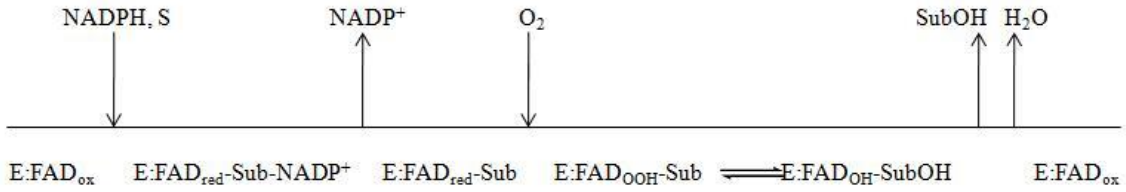

(B) mFMO, PAMO and PvdA

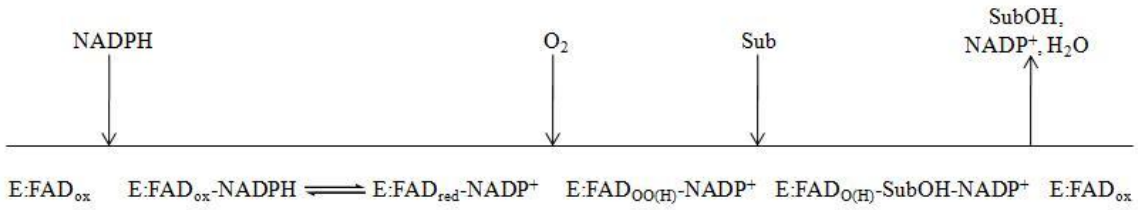

Figure 3.8. Schematic representations of mechanisms consistent with PHBH, mFMO, PAMO, and PvdA. **(A)** PHBH from *P. fluorescens*, **(B)** FMO from hog liver microsomes, PAMO from *Thermobifida fusca*, and PvdA from *P. aeruginosa*. The flavin states are labeled as oxidized (FAD_{ox}), reduced (FAD_{red}), hydroperoxyflavin intermediate (FAD_{HOOH}), and hydroxyflavin intermediate (FAD_{HOH}).

CHAPTER FOUR

Conformation and Catalysis

I. Introduction

Although globular proteins are generally closely-packed, they have certain degrees of flexibility. Most enzymes are inherently dynamic and usually require one or more conformational changes for catalysis to occur. In some instances, an entire protein domain may rotate or fold about its axis during catalysis. Still, others may only require that a single amino acid or cofactor alter its three-dimensional position to ensure turnover [75]. The dynamics involved during catalysis of enzymes can include changes upon binding of ligands or substrates, prevention of hydrophobic regions exposed to solvent, and directing cellular localization [75]. For purposes of this chapter, the dynamics involved in catalysis upon binding of ligands and substrates with respect to flavin-dependent enzymes will be discussed.

The flavin-dependent monooxygenases utilize a general cycle in which NADPH reduces FAD, and the reduced flavin then reacts with molecular oxygen to form a C4a-(hydro)peroxyflavin intermediate, which is the oxygenating agent. This complicated catalytic process has diverse requirements that is often difficult to satisfy at a single site [76]. Ballou and co-workers reviewed the two general strategies that have evolved to satisfy these requirements. First, PHBH is the paradigm for single-component flavoprotein monooxygenases and this enzyme undergoes significant protein and flavin dynamics during catalysis. There is an "out" conformation that gives access of substrate and product to solvent, and an "in" conformation for the reaction with oxygen and the hydroxylation to occur. The "out" conformation is achieved by movement of the

isoalloxazine ring toward the solvent, which exposes its N5 for hydride delivery from NADPH. Next, this "in" form prevents solvent from destabilizing the C4a-hydroperoxyflavin intermediate. The protein coordinates these dynamic events during catalysis [76].

The second strategy uses a reductase to catalyze the reduction of the flavin and an oxygenase that uses the reduced flavin as a substrate to react with oxygen and hydroxylate the organic substrate. One such example is *p*-hydroxyphenylacetate 3-hydroxylase (HPAH), from *E. coli* [77]. These two-component systems are able to transfer reduced flavin from the reductase to the oxygenase and stabilize the C4a-peroxyflavin until a substrate binds to be hydroxylated, all before flavin oxidation and release of H_2O_2. Again, protein dynamics are important for catalytic success [76].

Current structural studies of the L-ornithine N^5-oxygenases are hindered due to the lack of a known three-dimensional structure. Therefore, alternative means are needed to elucidate the conformational changes that *Af* SidA and others undergo during catalysis. That these enzymes contain two motifs for binding FAD and NADPH, it is likely structural rearrangements occur during coenzyme binding, flavin reduction and/or product release. As such, it is the focus of this chapter to examine protein dynamics in *Af* SidA in the presence and absence of its substrates.

II. Materials and Methods

4.2.1 Circular dichroism (CD) spectroscopy

Estimations of the secondary structure of *Af* SidA were performed using a Jasco J-720 spectropolarimeter (Easton, MD). *Af* SidA (1.06 µM final) was diluted to a final volume of 500 µL with a buffer consisting of 10 mM phosphate, 50 mM potassium fluoride, pH 7.5, within a cuvette (0.1 cm pathlength) supplied by the manufacturer. Measurements were recorded at 25^{o}C under a nitrogen gas atmosphere. Scans were performed from 260 – 190 nm, with 100 mdeg sensitivity, 1 sec response and an accumulation of three scans per sample were averaged and the experiments were replicated. For calibration, scans were performed in the presence of air, dd H_2O, the experimental buffer, as well as known concentrations of NAD^+ and $NADP^+$. Data analysis was performed using DiChroWeb licensed software available online [78].

4.2.2 Limited proteolysis analyses

To assess the effect of conformational changes in *Af* SidA induced by ligands, the protein (8.73 µM final) was diluted to a final volume of 200 µL with 100 mM HEPES, 125 mM NaCl, pH 7.5 buffer, along with either 5 mM $NAD(P)^+$, 15 mM L-ornithine or a combination of these substrates at 37^{o}C. At specific time intervals, aliquots (15 µL) were removed and immediately heated to 95^{o}C to quench the reaction. Sodium dodecyl sulfate-polyacrylamide gel electrophoresis (SDS-PAGE) was performed as described by Laemmli on 12% polyacrylamide gels [79].

4.2.3 Oxidized coenzyme titrations

In a 1 mL reaction, the spectrophotometer was scanned with 965 μL of buffer (100 mM phosphate, pH 7.5), which served as the blank. 20 μL of *Af* SidA were then added to the cuvette and a spectrum of the oxidized enzyme was recorded. Using a cuvette mixer, aliquots of $NADP^+$ were added to the reaction mixture and spectra of each $NADP^+$ concentration were recorded.

III. Results

4.3.1 CD spectroscopy

In the absence of ligand, the CD spectrum of *Af* SidA demonstrated significant negative peaks around 220 – 210 nm and 190 – 185 nm, indicating that roughly 50% of *Af* SidA is composed of α helices and anti-parallel β sheets [75] (Table 4.1). The secondary structure content of *Af* SidA appeared to change slightly in the presence either $NADP^+$ or NAD^+ (Figure 4.1). Important to note is that upon the addition of either coenzyme, the helix content decreased, while the turns and unordered contents increased. This suggests that *Af* SidA undergoes changes in its secondary structure to accommodate these ligands.

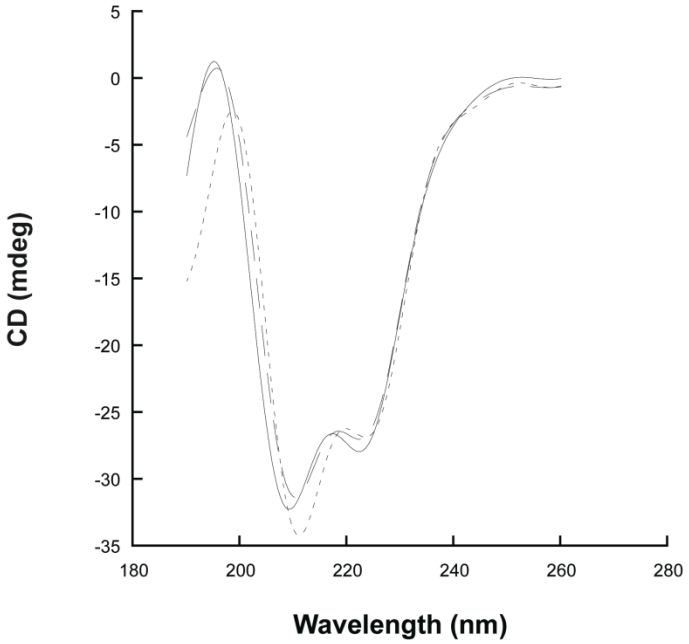

Figure 4.1. Circular dichroism spectra of *Af* SidA in the presence of ligands. *Af* SidA was scanned from 190 – 250 nm in the absence (—) or presence of 100 μM $NADP^+$ (---) or 100 μM NAD^+ (– –) at 25°C.

Table 4.1. Secondary structure comparisons among flavin monooxygenases

Sample	% Helix	% Sheet	% Coil	% Identity
FMO (*Methylophaga* sp. strain SK1)	25.1	29.9	45	12.2
PAMO (*T. fusca*)	31.5	22.3	46.2	13.2
Af SidA	29.5	20.3	50.2	-
+ $NADP^+$	25.8	23.6	55.5	-
+ NAD^+	26.9	20.3	54.5	-

4.3.2 Oxidized coenzyme titrations

The steady-state inhibition experiments with $NADP^+$ mentioned earlier indicated that the release of the oxidized coenzyme is the ultimate step in the catalytic cycle of *Af* SidA since it acts as a competitive inhibitor as a function of NADPH concentration. To gain insight into the process of $NADP^+$ release, the reverse reaction was monitored, i.e., the binding of the oxidized coenzyme to oxidized *Af* SidA, by measuring spectral changes of the flavin upon titration of 90 μM *Af* SidA with 0 – 30 μM $NADP^+$ (Figure 4.2). Evidence for several distinct spectral changes was observed at 385 nm and 500 nm. At both wavelengths, binding of $NADP^+$ resulted in absorbance shifts toward shorter wavelengths. Such spectral effects hint about changes in the microenvironment surrounding the flavin upon coenzyme binding.

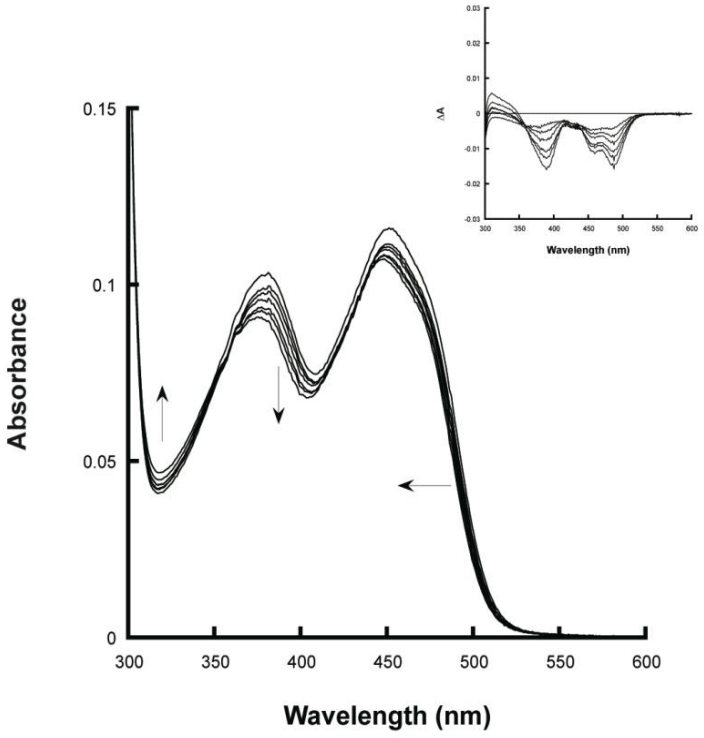

Figure 4.2. Spectral changes of *Af* SidA upon titration of $NADP^+$. Flavin absorbance spectra of *Af* SidA were recorded upon titration with $NADP^+$. The inset shows the difference spectra of *Af* SidA upon titration with $NADP^+$ using the spectrum of *Af* SidA with no $NADP^+$ as a reference.

4.3.3 Limited proteolysis analyses

Treatment of *Af* SidA with trypsin resulted in its rapid degradation. Similar studies performed in the presence of $NADP^+$ revealed the absence of such adverse action by the protease as indicated by a significant retention of the structural integrity of *Af* SidA (Figure 4.3). Further investigations over a range of $NADP^+$ concentration indicated that a coenzyme concentration of 5 mM was adequate to protect *Af* SidA from proteolytic degradation. Interestingly, NAD^+ (5 mM) was not found to shield *Af* SidA from tryptic digestion as indicated by similar degradation patterns of the enzyme in the absence of ligand. The other participant in the catalytic cycle of *Af* SidA, L-ornithine (15 mM), was also ineffective in preventing the enzyme from degradation by trypsin. Furthermore, when combined with $NADP^+$ (5 mM), the pattern of degradation resembled that of $NADP^+$ alone, suggesting that L-ornithine does not induce conformational changes during the catalytic cycle. It should also be noted that the protective effect exerted by $NADP^+$ does not appear to be due to the ability to function as an inhibitor of trypsin since Dick and co-workers report that these compounds have no adverse effect in experiments with azocasein serving as a substrate [80].

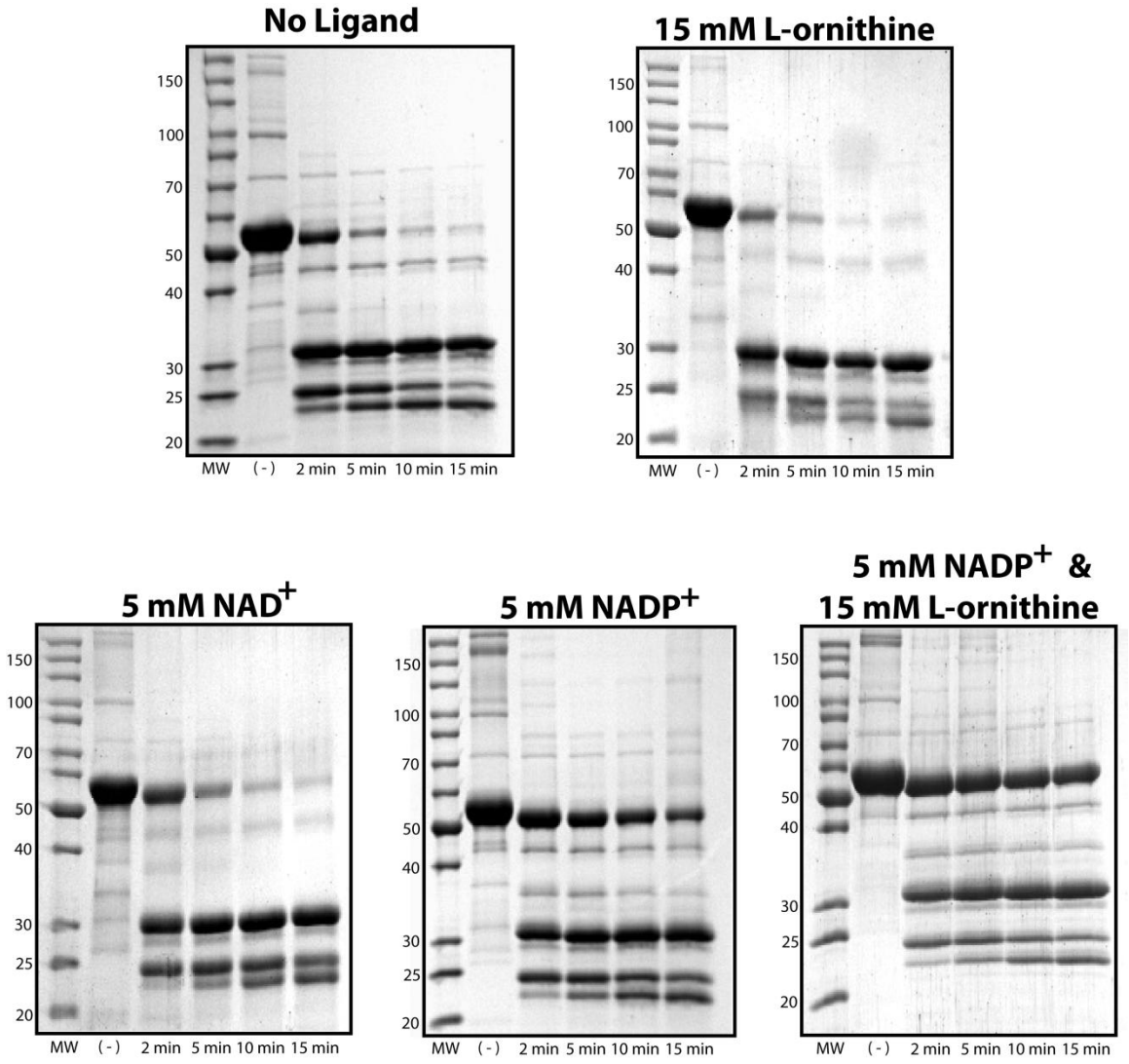

Figure 4.3. Trypsin digests of *Af* SidA in the presence of various ligands. *Af* SidA (5 mg mL^{-1}) was digested with trypsin (0.0001 mg mL^{-1}) in the presence of various ligands at 37^{o}C.

4.3.4 Trypsin cleavage patterns of *Af* SidA

Trypsin predominantly cleaves proteins at the carboxyl side of the amino acids lysine and arginine, except when either is followed by a proline [81]. Therefore, using mass spectroscopy, a map of the trypsin cleavage pattern was generated (Figure 4.4). It is shown that the protein band designated "2" is cleaved from *Af* SidA within two minutes of the initiation of the reaction. This protein band corresponds to residues 1 – 300, which includes both the FAD- and NADPH-binding domains of the protein. At the same time, a second, lower molecular weight band appears and is designated "3." This band corresponds to residues 301 – 501. Finally, after several minutes, the appearance of another band, designated "4," appears and corresponds to the cleavage of residues 490 – 501 from band "2."

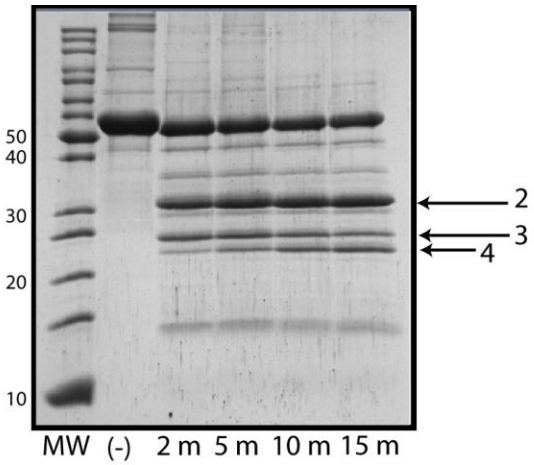


```
  1 MESVERKSES SYLGMRNMQP EQRLSLDPPR LRSTPQDELH DLLCVGFGPA
 51 SLAIAIALHD ALDPRLNKSA SNIHAQPKIC FLERQKQFAW HSGMLVPGSK
101 MQISFIKDLA TLRDPRSSFT FLNYLHQKGR LIHFTNLSTF LPARLEFEDY
151 MRWCAQQFSD VVAYGEEVVE VIPGKSDPSS SVVDFFTVRS RNVETGEISA <-- 2
201 RRTRKVVIAI GGTAKMPSGL PQDPRIIHSS KYCTTLPALL KDKSKPYNIA
251 VLGSGQSAAE IFHDLQKRYP NSRTTLIMRD SAMRPSDDSP FVNEIFNPER
301 VDKFYSQSAA ERQRSLLADK ATNYSVVRLE LIEEIYNDMY LQRVKNPDET
351 QWQHRILPER KITRVEHHGP QSRMRIHLKS SKPESEGAAN DVKETLEVDA <-- 3
401 LMVATGYNRN AHERLLSKVQ HLRPTGQDQW KPHRDYRVEM DPSKVSSEAG
451 IWLQGCNERT HGLSDSLLSV LAVRGGEMVQ SIFGEQLERA AVQGHQLRAM <-- 4
501 L
```

Figure 4.4. Mass spectral analysis of proteolyzed *Af* SidA. Bands corresponding to specific molecular weights were analyzed by MALDI-TOF MS to identify specific cleavage patterns.

IV. Discussion

The conformational changes in *Af* SidA accompanying its interaction with its ligands were assessed by examining the CD spectra, its susceptibility to degradation by trypsin, and titration with $NADP^+$. With regard to both the CD spectra and $NADP^+$ titration, the profile of *Af* SidA was affected in the presence of its cofactors. In addition, its susceptibility to the action of trypsin was found to be influenced by the presence of some of its ligands; the details are given below.

4.4.1 Ligand-induced conformational changes using CD and UV/Vis spectroscopy

Results from this chapter revealed that the substrate L-ornithine does not induce significant conformational changes in *Af* SidA. Yet, the coenzymes $NADP^+$ and NAD^+ did exert changes in *Af* SidA that help explain how this enzyme can utilize both coenzymes during catalysis. However, the severity of change is markedly different between the two. With respect to differences in the circular dichroism (CD) spectra, the effects of coenzyme binding are evident between $NADP^+$ and NAD^+ (Table 4.1). Here, it was seen that $NADP^+$ causes a more severe change in the helix, strand and turns content than did NAD^+. This discrepancy is likely a result of the differences in binding affinities for each coenzyme. As mentioned in the previous chapter, the oxygen consumption assay demonstrated a 7-fold higher K_m for NADH than for NADPH. The results from this experiment strengthen the argument that, although *Af* SidA utilizes both cofactors during catalysis, NADPH couples the reaction more efficiently, thus preventing hydrogen peroxide formation.

The secondary structure content of *Af* SidA was also compared to the known crystal structures of functionally related flavin-containing monooxygenases. Table 4.1 provides the secondary structure content of *Af* SidA compared to FMO from *Methylophaga* sp. strain SK1 and PAMO [82, 83]. These results show that although the percent identity between *Af* SidA and these monooxygenases is low, the relative amounts of secondary structure content are comparable. In a separate study, the primary amino acid sequence of *Af* SidA was submitted to the Protein Homology/Analogy Recognition Engine (PHYRE), which compares a given sequence to the database of known crystal structures [84]. Therefore, homology modeling is possible even without a known three-dimensional structure of a protein. Results from this experiment showed that the amino acid sequence of *Af* SidA is most likely structurally related to the aforementioned phenylacetone monooxygenase (data not shown), which is consistent with the similarities among the kinetic mechanisms of these two enzymes.

Experiments where *Af* SidA was titrated with increasing concentrations of $NADP^+$ further demonstrate changes occurring in the active site of the enzyme. It was shown that, as the coenzyme concentration increases, perturbations are observed in the flavin spectra. These spectral shifts indicate that the microenvironment of the flavin was changing as a result of $NADP^+$ binding. In support of this argument, Pazmiño and co-workers observed similar effects when elucidating the kinetic mechanism of PAMO [74]. In this report, they noted that binding of $NADP^+$ resulted in a more resolved flavin spectrum, which suggests a change in the environment around the flavin. This statement is in line with the bound nicotinamide ring of $NADP^+$ shielding the flavin from water [74]. This may also be the case with *Af* SidA, since experiments have shown that the

enzyme is stabilized only in the presence of salts, which likely influence the hydrophobicity of the flavin environment (discussed in the following chapter).

4.4.2 Ligand-induced conformational changes measured through limited proteolysis

When susceptibility to degradation by trypsin was employed as a method for monitoring the structural changes in *Af* SidA, significant differences in the response due to interaction with its various ligands and substrate became apparent. *Af* SidA, in the absence of its coenzyme or substrate, was susceptible to rapid degradation by trypsin. Conversely, such adverse action of trypsin was significantly inhibited when experiments were performed in the presence of $NADP^+$ (5 mM). The other ligands examined, NAD^+ (5 mM) and L-ornithine (15 mM) were not found to confer any additional protection from proteolysis. L-ornithine, its required substrate, does not afford protection, which is probably due to its inability to induce any conformational change in the enzyme. It is likely that L-ornithine enters the active site of the enzyme after binding of the coenzyme and locates itself in close proximity to the flavin cofactor, without perturbing the orientation of the peroxyflavin, consistent with the rates of oxygen consumption by Af SidA in the presence and absence of its substrate (Table 3.2).

Under similar conditions performed with L-ornithine present, NAD^+ was similarly ineffective in preventing the proteolysis of *Af* SidA. This was unusual, since it was observed that NAD^+ binding induced changes in the secondary structure of the enzyme, in addition to *Af* SidA being able to utilize this cofactor during catalysis (Tables 3.1 and 4.1). The reason NAD+ doe not afford protection from proteolysis is not clear; this finding may be a reflection of the structural difference between NADH and NADPH.

Since NADH lacks the 2'-phosphate on its ribose ring, this excludes certain interactions between this coenzyme and its putative binding pocket. As a result, NADH locates into the same site as NADPH during catalysis, however, it is ineffective at coupling flavin reduction with oxygen consumption. Figure 3.6 illustrates that this lack of conformational change leads to increased levels of hydrogen peroxide formation.

4.4.3 The moonlighting role of NADPH in catalysis

The well known role of NADPH during catalysis of flavin-dependent monooxygenases is to provide reducing equivalents to FAD. The chemistry of NADPH requires that reduction of the flavin cofactor is brought about through a hydride transfer from the C4 atom of the nicotinamide ring to the flavin N5 atom [82]. Bound $NADP^+$ has been shown to play other roles during catalysis. For example, Alfieri and co-workers demonstrated that $NADP^+$ not only provides reducing equivalents to the flavin during turnover of FMO (*Methylophaga* sp. strain SK1), but that $NADP^+$ also stabilized the C4a-hydroperoxyflavin for several minutes [82]. In fact, this report explained that similar to mFMO (hog liver microsomes), the bacterial enzyme behaves like a "cocked gun," spending most of the time in the form of the hydroperoxyflavin intermediate [82]. Strikingly similar was the behavior of *Af* SidA. In this study, it was shown that *Af* SidA readily utilized NADPH for reducing equivalents; limited proteolysis experiments provided physical evidence of conformational changes induced by coenzyme binding, and *Af* SidA formed and stabilized the C4a-(hydro)peroxyflavin intermediate. Taken together, this study provides direct evidence for the preference of NADPH over NADH by *Af* SidA.

4.4.4 Determining *Af* SidA cleavage patterns

Lastly, the cleavage pattern of *Af* SidA was important to fully understand the dynamics involved during catalysis. In these experiments, it was demonstrated that introduction of the protease resulted in the rapid formation of two bands estimated at 31 kDa and 27 kDa, which corresponded to residues 1 – 300 and 301 – 501of *Af* SidA, respectively (Figure 4.4). As the incubation period increased, a third band appeared, corresponding to ~26 kDa and represented the cleavage of residues 490 – 501 from the 27 kDa band. By mapping the pattern of proteolysis, it was possible to predict the degradation behavior of the enzyme. First, the appearance of band 2 includes both the FAD- and NADPH-binding domains of *Af* SidA, which are essential for catalysis. Furthermore, the cleavage of *Af* SidA at R300 may hint at the domain orientation of the enzyme. The portion of the enzyme containing the first 300 residues may be a tightly packed region, whereas other portions of *Af* SidA could be less tightly packed and thus available for proteolysis. Secondly, the cleavage of the final twelve residues from the remaining peptide may also be a result of the quaternary structure of *Af* SidA. Interestingly, it was shown by Dick and co-workers that the functional homolog IucD suffered a loss of structural stability and complete loss of monooxygenase function when this same region of the peptide was removed. It was reported that this region of IucD may play a role in the maintenance of IucD in its catalytically active conformation [80]. It would be interesting if similar effects are observed when *Af* SidA is tested under parallel conditions.

CHAPTER FIVE

Inhibition by Halides and Phenylglyoxal

I. Introduction

The catalytic function of several flavin-dependent monooxygenases, including PHBH, is adversely affected by monovalent anions. In the case of PHBH, Steennis and co-workers demonstrated that the inhibitory action of chloride was likely due to its ability to compete for the NADPH-binding site, therefore disrupting ionic interactions and resulting in decreased enzyme efficiency [85]. Later, Gatti and co-workers determined from the crystal structure of PHBH that the enzyme contains several chloride binding sites, one of which interferes with flavin intermediate formation and substrate hydroxylation [86]. In contrast, the L-lysine N^6-oxygenase, IucD, was reported to be most active with an increased chloride concentration (50 mM) [87]. Therefore, the preference of ion concentrations by related enzymes can vary dramatically and it is necessary to understand these criteria in order to provide an accurate biochemical analysis.

As previously mentioned, there is no known three-dimensional structure for any member of the N-hydroxylating monooxygenases (i.e., PvdA, VbsO, IucD, *Af* SidA). Since this information is not available yet, investigation of the active site topography has been performed mainly by the use of specific chemical modifiers or artificial flavins [67]. However, *Af* SidA catalyzes the hydroxylation of L-ornithine, an amino acid containing a carboxyl group. It has been documented that other flavoproteins bind substrates with a similar carboxyl group utilizing arginine guadinium groups to ion pair at the protein's

active site [88]. Therefore, it was decided to test the role of arginine residues in *Af* SidA through the use of an arginine-reactive compound, phenylglyoxal.

In this chapter, the effects of various halides on the activity of *Af* SidA are reported, including results from oxygen consumption and product formation assays. Furthermore, the reactivity of arginine residues in *Af* SidA are assessed to better understand the roles of particular residues in catalysis.

II. Materials and Methods

5.2.1 Inhibition assays by halides

Unless otherwise specified, the reaction conditions were 2 μM *Af* SidA in 100 mM phosphate, pH 7.5 buffer with 0.5 mM NADPH and 15 mM L-ornithine. To introduce the various halides into the reaction mixture, buffers containing 100 mM phosphate were combined with increasing concentrations of KBr, NaCl, KF or KI. At different times, 104 μL aliquots of the reaction mixture were withdrawn and assayed using the product assay. Buffers containing the increased halide concentrations were also used for the oxygen consumption assay, which was performed as described in chapter 3.

5.2.2 Inhibition of *Af* SidA by phenylglyoxal

To assess the reactivity of arginine guadinium groups of *Af* SidA with phenylglyoxal, an initial reaction mixture was composed of buffer (100 mM phosphate, pH 7.5), *Af* SidA (2.0 μM), and L-ornithine (15 mM) in the presence of various concentrations of phenylglyoxal (0 to 9 mM) in a final volume of 700 μL. At specific time intervals, 92 μL aliquots were removed and mixed with 1 mM NADPH to initiate

turnover. Activity measurements were performed according to the product formation assay described above.

III. Results

5.3.1 Inhibition of *Af* SidA by halides

Af SidA demonstrated that it required a critical ion concentration for stability and optimum activity. Depending on the halide, however, the activity of the enzyme was also inhibited to different extents. For example, the inhibition of *Af* SidA was monitored using increasing chloride concentrations and assessed by the product formation assay (Table 5.1). Double-reciprocal plots revealed a series of parallel lines, consistent with chloride being an uncompetitive inhibitor against L-ornithine. The inhibition constants calculated were 1800 ± 20 μM (K_{IS}) and 115 ± 22 mM (K_{II}).

In separate experiments, the effects of halides on oxygen consumption for *Af* SidA were monitored (Table 5.2). In the presence of 250 mM halide salt, the rate of oxygen consumption decreased only slightly with fluorine serving as the halide. Conversely, chlorine, bromine, and iodine each significantly inhibited the enzyme, ranging from 27 – 90 % inhibition. Furthermore, the effects on product formation were also examined in the presence these halides. Table 5.3 shows IC_{50} values calculated based upon data from the product formation assays. Similar to the oxygen consumption assay, fluorine exerted little or no inhibitory effects. Chlorine, on the other hand, inhibited product formation and an IC_{50} value of 500 ± 1.2 mM was calculated. As expected, bromine and iodine, were especially deleterious and the IC_{50} values calculated were 50 ± 13 mM and 25 ± 12 mM, respectively.

5.3.2 Inhibition of *Af* SidA by phenylglyoxal

When subjected to the arginine-specific reactant, phenylglyoxal, *Af* SidA exhibited time-dependent inactivation (Figure 5.2). A replot of the slope of each line from **(A)** versus inhibitor concentration lead to the calculation of an inactivation rate of $188 \pm 123\ \mu M\ min^{-1}$.

Table 5.1. Inhibition of *Af* SidA by chloride.

Inhibitor	Varied Component	Type of Inhibition [4]	K_{IS}, μM	K_{II}, mM
Chloride	L-ornithine	uncompetitive	1800 ± 20	115 ± 22

[4]Equation is provided in Materials and Methods of chapter 3.

Table 5.2. Effect of halides on oxygen consumption.

Test condition	% Relative Activity
100 mM phosphate, pH 7.5	100
+ 250 mM KF	96
+ 250 mM NaCl	73
+ 250 mM KBr	33
+ 250 mM KI	10

Table 5.3. IC_{50} values of various halides.

Halide	IC_{50}, mM [5]	Atomic radius, pm[3]
Fluorine	*A*	50
Chlorine	500 ± 1.2	100
Bromine	50 ± 13	115
Iodine	25 ± 15	140

[5] Equation provided in the Materials and methods of chapter 3.

[a] < 10% inhibition at 1 M halide.

5.3.2 Inhibition of *Af* SidA by phenylglyoxal

When subjected to the arginine-specific reactant, phenylglyoxal, *Af* SidA exhibited time-dependent inactivation (Figure 5.2). A replot of the slope of each line from **(A)** versus inhibitor concentration provided a rate of inactivation, 188 ± 123 μM min^{-1}.

IV. Discussion

5.4.1 Inhibitory effects of halides

The inhibitory effects exerted by the halides bromine, chlorine, fluorine, and iodine on *Af* SidA were determined. During preparations of the enzyme, it was found that *Af* SidA required at least 50 mM NaCl to maintain its structural integrity, as well as effectively bind its FAD cofactor. Therefore, initial biochemical assays performed consisted of a buffer containing at least 125 mM NaCl. This led to inhibition of the enzyme, and required that all subsequent assays utilize a buffer with no chloride ions. Of the buffers tested, it was found that 100 mM phosphate, pH 7.5, maintained both the integrity of the flavin environment and provided steady-state kinetic parameters that were comparable to other members of the N-hydroxylating monooxygenases.

To gain insight into the inhibition of *Af* SidA by halides, the relative activities in the presence of the halides were compared to their atomic radii (Table 5.3). It is shown that as the radius of the ion increases, so too does its inhibitory effect. This suggests that, although each halide can enter the active site, there reaches a certain size where the ions either disrupt the flavin environment or interfere with electrostatic interactions of the protein.

5.4.2 Inhibition by chloride

In this chapter, results demonstrate that *Af* SidA required a minimum concentration of salt ions to maintain its structural integrity and catalytic activity. The introduction of excess chloride ions to both the purification buffers and assay buffers resulted in a stable and active *Af* SidA enzyme. On the other hand, it was observed through the product formation and oxygen consumption assays that the putative benefits from chloride ions were counteracted by their inhibitory action (Tables 5.1 – 5.3). With respect to the structure of *Af* SidA, it can be proposed that certain ionic interactions are required for stability. Moreover, separate experiments demonstrated that even at 500 mM NaCl, the absorption spectrum of the enzyme was not affected (data not shown). However, concentrations greater than ~50 mM NaCl inhibited the catalytic function, presenting a difficult situation to properly characterize the enzyme. The results from Table 5.1 may indicate that L-ornithine and chloride both bind at the active site, but chloride probably binds to a second site leading to this inhibition pattern. This observation is not unusual as it has also been documented with other N-hydroxylating monooxygenases. Specifically, similar inhibition patterns by PvdA were observed, albeit the inhibitory concentrations were significantly lower [58].

5.4.2 Inhibition by phenylglyoxal

In this chapter, results demonstrate that *Af* SidA was inactivated by the arginine-specific inhibitor, phenylglyoxal, PGO (Figure 5.2). Because PGO is an arginine-specific reactant, structural information could be gathered as to the reactivity of accessible guadinium groups. Although the exact number of reactive arginines was not calculated in

these experiments, it can be concluded that there exists at least one arginine group involved in catalysis of *Af* SidA. This residue could possibly play a role in stabilizing a specific ion pair at the active site or even an oxygenated flavin intermediate.

Roles for the participation of arginine residues during catalysis were examined by Malito and co-workers while elucidating the structure of PAMO [83]. Inspection of the crystal structure of PAMO revealed that residue R337 was positioned close to the flavin cofactor, where it assisted in the formation and stabilization of the C4a-peroxyflavin. In a separate report, the R337K and R337A mutants were still capable of stabilizing the flavin intermediate, however, they were unable to form product. This demonstrated that this arginine was critically involved during catalysis [74]. Using online structural modeling software, in conjunction with PyMol molecular viewing software, the amino acid sequence of *Af* SidA was threaded onto the three-dimensional structure of the aforementioned phenylacetone monooxygenase crystal structure. A conserved arginine residue (R363) in *Af* SidA was located in an almost identical location to that of R337 [84, 89]. It is hypothesized that the R363 in *Af* SidA may be the site of phenylglyoxal reaction. Site-directed mutagenesis could be one tool to monitor changes in the stabilization of the peroxyflavin in *Af* SidA.

(A)

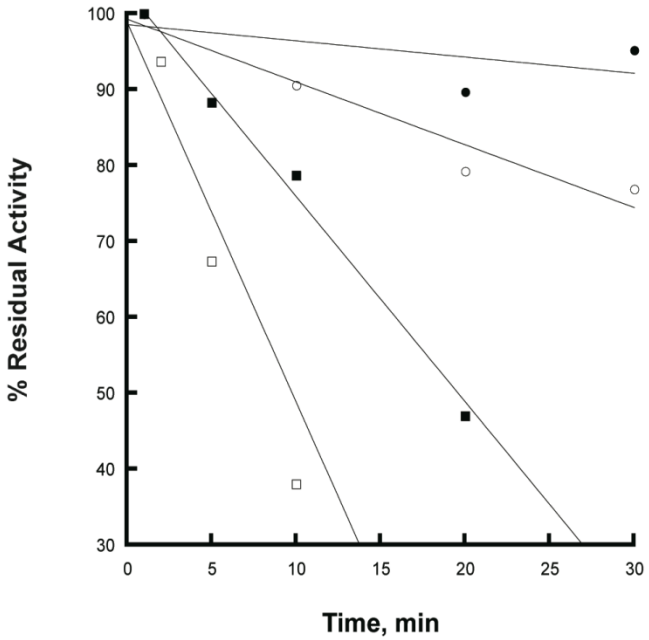

(B)

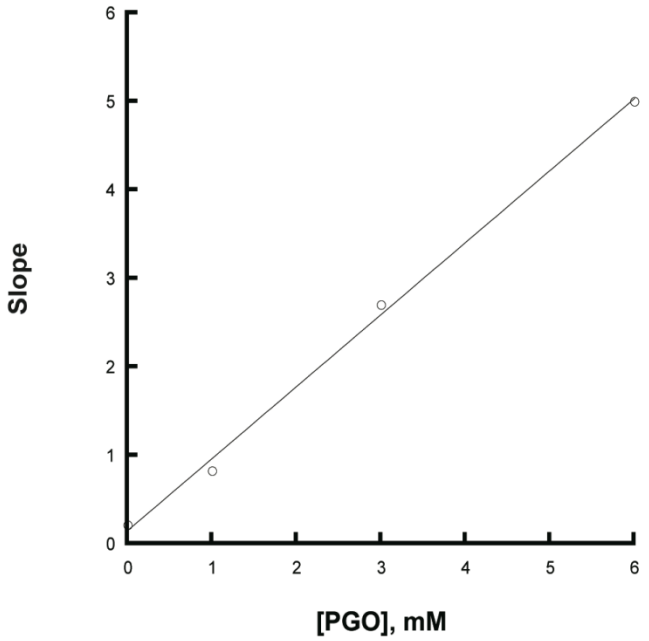

Figure 5.1. Inhibition of *Af* SidA by phenylglyoxal. **(A)** The time-dependent inactivation of *Af* SidA. Phenylglyoxal concentrations used were (●) 0mM, (○) 1 mM, (■) 3 mM, and (□) 6mM. **(B)** Replot of slopes versus phenylglyoxal concentration.

CHAPTER SIX

CONCLUDING REMARKS

Iron is essential for nearly all living organisms. However, the bioavailability of iron is diminished due to its rapid oxidation in aerobic environments. In response to infection, mammalian hosts decrease available iron concentrations to essentially starve the invaders. Microbes employ a variety of systems to circumvent these defenses and satisfy their iron requirements. One such mechanism is the biosynthesis and secretion of low molecular weight molecules with high iron affinity, termed siderophores. After sequestering iron, these Fe^{3+}-bound siderophores are then transported back to the microbe, where elemental iron participates in a variety of biological reactions.

Nature seems to have tailored amino acid precursors, such as lysine and ornithine, to serve as a site of iron ligation in siderophore scaffolds. The derivitized molecules, containing a hydroxamate moiety, have the ability to capture ferric iron through a network of coordinated linkages. As part of an effort to understand the origin and role of N-hydroxylation in the transformation of readily available amino acids into nonribosomal peptides and related small molecules, this study investigated one fungal strategy for L-ornithine tailoring in the context of the siderophore ferrichrome. Using recombinant expression, the *Aspergillus fumigatus* SidA, catalyzing the hydroxylation of the terminal amine from L-ornithine, was expressed in *E. coli* cells and purified to homogeneity. This is the first report of an NMO purified with a tightly bound FAD cofactor. This set the stage for a detailed biochemical characterization of the poorly understood siderophore biosynthetic enzyme.

The investigation of *Af* SidA began by determining its steady-state kinetic parameters, including apparent catalytic rates, as well as apparent substrate binding affinities and coenzyme specificities. The enzyme undergoes two half-reactions where FAD is first reduced. The flavin cofactor then activates molecular oxygen, wherein the substrate is later hydroxylated. These two reactions were characterized separately through use of the product formation and oxygen consumption assays. Here, it was revealed that *Af* SidA is site-specific for the distal nitrogen in L-ornithine, but is promiscuous with respect to its utilization of reducing equivalents. Closer examination revealed that *Af* SidA prefers NADPH versus NADH due to a lower apparent binding affinity and decreased hydrogen peroxide formation.

Studies of the ligand-induced conformational changes were also used as a tool to probe the dynamic nature of *Af* SidA during catalysis. These experiments demonstrated that after binding, $NADP^+$ induces both changes in the secondary structure and prevents degradation by trypsin. Of the other participants, neither NAD^+ nor its substrate, L-ornithine, created any conformational rearrangements and were ineffective at preventing proteolysis. Finally, the halides bromine, chlorine, fluorine, and iodine each exerted inhibitory effects on both oxygen consumption and product formation by *Af* SidA. In addition, chloride was found to be an uncompetitive inhibitor of the enzyme with respect to its substrate. Separate experiments demonstrated a role for arginine residues during catalysis, as *Af* SidA was inhibited by the guadinium-reactive compound, phenylglyoxal.

This report provides preliminary data that will assist in future studies, including the elucidation of the kinetic mechanism of *Af* SidA, site-directed mutagenesis studies

and determining the three-dimensional structure, for which crystals have already been obtained (data not shown).

REFERENCE LIST

1. Pierre, J.L. and M. Fontecave, *Iron and activated oxygen species in biology: the basic chemistry.* Biometals, 1999. **12**(3): p. 195-9.

2. Maton, A., editor, *Human Biology and Health.* 1993, Englewood Cliffs, New Jersey, USA: Prentice Hall.

3. Meunier, B., S.P. de Visser, and S. Shaik, *Mechanism of oxidation reactions catalyzed by cytochrome p450 enzymes.* Chem Rev, 2004. **104**(9): p. 3947-80.

4. Chelikani, P., I. Fita, and P.C. Loewen, *Diversity of structures and properties among catalases.* Cell Mol Life Sci, 2004. **61**(2): p. 192-208.

5. Gaetani, G.F., et al., *Predominant role of catalase in the disposal of hydrogen peroxide within human erythrocytes.* Blood, 1996. **87**(4): p. 1595-9.

6. Hassett, D.J., et al., *Quorum sensing in Pseudomonas aeruginosa controls expression of catalase and superoxide dismutase genes and mediates biofilm susceptibility to hydrogen peroxide.* Mol Microbiol, 1999. **34**(5): p. 1082-93.

7. McCord, J.M. and I. Fridovich, *Superoxide dismutase: the first twenty years (1968-1988).* Free Radic Biol Med, 1988. **5**(5-6): p. 363-9.

8. Naranuntarat, A., et al., *The interaction of mitochondrial iron with manganese superoxide dismutase.* J Biol Chem, 2009. **284**(34): p. 22633-40.

9. Leahy, J.G., P.J. Batchelor, and S.M. Morcomb, *Evolution of the soluble diiron monooxygenases.* FEMS Microbiol Rev, 2003. **27**(4): p. 449-79.

10. Merkx, M., et al., *Dioxygen Activation and Methane Hydroxylation by Soluble Methane Monooxygenase: A Tale of Two Irons and Three Proteins A list of abbreviations can be found in Section 7.* Angew Chem Int Ed Engl, 2001. **40**(15): p. 2782-2807.

11. Fox, B.G., et al., *Stearoyl-acyl carrier protein delta 9 desaturase from Ricinus communis is a diiron-oxo protein.* Proc Natl Acad Sci U S A, 1993. **90**(6): p. 2486-90.

12. Fischbach, M.A., et al., *How pathogenic bacteria evade mammalian sabotage in the battle for iron.* Nat Chem Biol, 2006. **2**(3): p. 132-8.

13. Raymond, K.N., E.A. Dertz, and S.S. Kim, *Enterobactin: an archetype for microbial iron transport.* Proc Natl Acad Sci U S A, 2003. **100**(7): p. 3584-8.

14. Andrews, S.C., A.K. Robinson, and F. Rodriguez-Quinones, *Bacterial iron homeostasis.* FEMS Microbiol Rev, 2003. **27**(2-3): p. 215-37.

15. Posey, J.E. and F.C. Gherardini, *Lack of a role for iron in the Lyme disease pathogen.* Science, 2000. **288**(5471): p. 1651-3.

16. Weinberg, E.D., *The Lactobacillus anomaly: total iron abstinence.* Perspect Biol Med, 1997. **40**(4): p. 578-83.

17. Schrettl, M., et al., *Siderophore biosynthesis but not reductive iron assimilation is essential for Aspergillus fumigatus virulence.* J Exp Med, 2004. **200**(9): p. 1213-9.

18. Blaser, M.J., *Helicobacter pylori and the pathogenesis of gastroduodenal inflammation.* J Infect Dis, 1990. **161**(4): p. 626-33.

19. Velayudhan, J., et al., *Iron acquisition and virulence in Helicobacter pylori: a major role for FeoB, a high-affinity ferrous iron transporter.* Mol Microbiol, 2000. **37**(2): p. 274-86.

20. Suzuki, T., et al., *Cytoplasmic ATPase involved in ferrous ion uptake from magnetotactic bacterium Magnetospirillum magneticum AMB-1.* FEBS Lett, 2007. **581**(18): p. 3443-8.

21. Neres, J., et al., *Aryl acid adenylating enzymes involved in siderophore biosynthesis: fluorescence polarization assay, ligand specificity, and discovery of non-nucleoside inhibitors via high-throughput screening.* Biochemistry, 2008. **47**(45): p. 11735-49.

22. Crosa, J.H. and C.T. Walsh, *Genetics and assembly line enzymology of siderophore biosynthesis in bacteria.* Microbiol Mol Biol Rev, 2002. **66**(2): p. 223-49.

23. Miethke, M. and M.A. Marahiel, *Siderophore-based iron acquisition and pathogen control.* Microbiol Mol Biol Rev, 2007. **71**(3): p. 413-51.

24. Stork, M., et al., *Two tonB systems function in iron transport in Vibrio anguillarum, but only one is essential for virulence.* Infect Immun, 2004. **72**(12): p. 7326-9.

25. Annamalai, R., et al., *Recognition of ferric catecholates by FepA.* J Bacteriol, 2004. **186**(11): p. 3578-89.

26. Buchanan, S.K., et al., *Crystal structure of the outer membrane active transporter FepA from Escherichia coli.* Nat Struct Biol, 1999. **6**(1): p. 56-63.

27. Faraldo-Gomez, J.D. and M.S. Sansom, *Acquisition of siderophores in gram-negative bacteria.* Nat Rev Mol Cell Biol, 2003. **4**(2): p. 105-16.

28. Lin, H., et al., *In vitro characterization of salmochelin and enterobactin trilactone hydrolases IroD, IroE, and Fes.* J Am Chem Soc, 2005. **127**(31): p. 11075-84.

29. Hantke, K., *Iron and metal regulation in bacteria.* Curr Opin Microbiol, 2001. **4**(2): p. 172-7.

30. Quadri, L.E., *Assembly of aryl-capped siderophores by modular peptide synthetases and polyketide synthases.* Mol Microbiol, 2000. **37**(1): p. 1-12.

31. Challis, G.L., *A widely distributed bacterial pathway for siderophore biosynthesis independent of nonribosomal peptide synthetases.* Chembiochem, 2005. **6**(4): p. 601-11.

32. Quadri, L.E., et al., *Identification of a Mycobacterium tuberculosis gene cluster encoding the biosynthetic enzymes for assembly of the virulence-conferring siderophore mycobactin.* Chem Biol, 1998. **5**(11): p. 631-45.

33. Johnson, L., *Iron and siderophores in fungal-host interactions.* Mycol Res, 2008. **112**(Pt 2): p. 170-83.

34. Heemstra, J.R., C.T. Walsh, and E.S. Sattely, *Enzymatic Tailoring of Ornithine in the Biosynthesis of the Rhizobium Cyclic Trihydroxamate Siderophore Vicibactin.* J Am Chem Soc, 2009. **131**: p. 15317 - 15329.

35. Thomas, G. *Tuberculosis*. 2007 [cited 2009 December 12]; Available from: http://www.who.int/mediacentre/factsheets/fs104/en/.

36. Raviglione, M.C. and I.M. Smith, *XDR tuberculosis--implications for global public health.* N Engl J Med, 2007. **356**(7): p. 656-9.

37. Zignol, M., et al., *Global incidence of multidrug-resistant tuberculosis.* J Infect Dis, 2006. **194**(4): p. 479-85.

38. Schrettl, M., et al., *Distinct roles for intra- and extracellular siderophores during Aspergillus fumigatus infection.* PLoS Pathog, 2007. **3**(9): p. 1195-207.

39. Tekaia, F. and J.P. Latge, *Aspergillus fumigatus: saprophyte or pathogen?* Curr Opin Microbiol, 2005. **8**(4): p. 385-92.

40. Greenberger, P.A., *Allergic bronchopulmonary aspergillosis.* J Allergy Clin Immunol, 2002. **110**(5): p. 685-92.

41. Marr, K.A., T. Patterson, and D. Denning, *Aspergillosis. Pathogenesis, clinical manifestations, and therapy.* Infect Dis Clin North Am, 2002. **16**(4): p. 875-94, vi.

42. Dasbach, E.J., G.M. Davies, and S.M. Teutsch, *Burden of aspergillosis-related hospitalizations in the United States.* Clin Infect Dis, 2000. **31**(6): p. 1524-8.

43. Lee, K.S., et al., *Treatment of hemoptysis in patients with cavitary aspergilloma of the lung: value of percutaneous instillation of amphotericin B.* AJR Am J Roentgenol, 1993. **161**(4): p. 727-31.

44. Ferreras, J.A., et al., *Small-molecule inhibition of siderophore biosynthesis in Mycobacterium tuberculosis and Yersinia pestis.* Nat Chem Biol, 2005. **1**(1): p. 29-32.

45. Sokol, P.A., et al., *Role of ornibactin biosynthesis in the virulence of Burkholderia cepacia: characterization of pvdA, the gene encoding L-ornithine N(5)-oxygenase.* Infect Immun, 1999. **67**(9): p. 4443-55.

46. Takase, H., et al., *Impact of siderophore production on Pseudomonas aeruginosa infections in immunosuppressed mice.* Infect Immun, 2000. **68**(4): p. 1834-9.

47. Hissen, A.H., et al., *The Aspergillus fumigatus siderophore biosynthetic gene sidA, encoding L-ornithine N5-oxygenase, is required for virulence.* Infect Immun, 2005. **73**(9): p. 5493-503.

48. Yeh, E., S. Garneau, and C.T. Walsh, *Robust in vitro activity of RebF and RebH, a two-component reductase/halogenase, generating 7-chlorotryptophan during rebeccamycin biosynthesis.* Proc Natl Acad Sci U S A, 2005. **102**(11): p. 3960-5.

49. Itoh, K., Z. Huang, and H.W. Liu, *Synthesis and analysis of substrate analogues for UDP-galactopyranose mutase: implication for an oxocarbenium ion intermediate in the catalytic mechanism.* Org Lett, 2007. **9**(5): p. 879-82.

50. Blazyk, J.L. and S.J. Lippard, *Expression and characterization of ferredoxin and flavin adenine dinucleotide binding domains of the reductase component of soluble methane monooxygenase from Methylococcus capsulatus (Bath).* Biochemistry, 2002. **41**(52): p. 15780-94.

51. Butler, C.S. and J.R. Mason, *Structure-function analysis of the bacterial aromatic ring-hydroxylating dioxygenases.* Adv Microb Physiol, 1997. **38**: p. 47-84.

52. Fitzpatrick, P.F., *Substrate dehydrogenation by flavoproteins.* Acc Chem Res, 2001. **34**(4): p. 299-307.

53. Massey, V., *The chemical and biological versatility of riboflavin.* Biochem Soc Trans, 2000. **28**(4): p. 283-96.

54. Ghisla, S. and V. Massey, *New flavins for old: artificial flavins as active site probes of flavoproteins.* Biochem J, 1986. **239**(1): p. 1-12.

55. Heuts, D.P., et al., *What's in a covalent bond? On the role and formation of covalently bound flavin cofactors.* FEBS J, 2009. **276**(13): p. 3405-27.

56. Draper, R.D. and L.L. Ingraham, *A potentiometric study of the flavin semiquinone equilibrium.* Arch Biochem Biophys, 1968. **125**(3): p. 802-8.

57. Garrett, R.H. and C.M. Grisham, *Biochemistry: Updated Third Edition*. 2007, Belmont, CA: Thomson Brooks/Cole.

58. Meneely, K.M. and A.L. Lamb, *Biochemical characterization of a flavin adenine dinucleotide-dependent monooxygenase, ornithine hydroxylase from Pseudomonas aeruginosa, suggests a novel reaction mechanism.* Biochemistry, 2007. **46**(42): p. 11930-7.

59. Ge, L. and S.Y. Seah, *Heterologous expression, purification, and characterization of an l-ornithine N(5)-hydroxylase involved in pyoverdine siderophore biosynthesis in Pseudomonas aeruginosa.* J Bacteriol, 2006. **188**(20): p. 7205-10.

60. Pohlmann, V. and M.A. Marahiel, *Delta-amino group hydroxylation of L-ornithine during coelichelin biosynthesis.* Org Biomol Chem, 2008. **6**(10): p. 1843-8.

61. Blommel, P.G., et al., *Enhanced bacterial protein expression during auto-induction obtained by alteration of lac repressor dosage and medium composition.* Biotechnol Prog, 2007. **23**(3): p. 585-98.

62. Plattner, H.J., et al., *Isolation and some properties of lysine N6-hydroxylase from Escherichia coli strain EN222.* Biol Met, 1989. **2**(1): p. 1-5.

63. van Berkel, W.J., N.M. Kamerbeek, and M.W. Fraaije, *Flavoprotein monooxygenases, a diverse class of oxidative biocatalysts.* J Biotechnol, 2006. **124**(4): p. 670-89.

64. Fraaije, M.W., et al., *Identification of a Baeyer-Villiger monooxygenase sequence motif.* FEBS Lett, 2002. **518**(1-3): p. 43-7.

65. Tomlinson, G., W.H. Cruickshank, and T. Viswanatha, *Sensitivity of substituted hydroxylamines to determination by iodine oxidation.* Anal Biochem, 1971. **44**(2): p. 670-9.

66. Hildebrandt, A.G., et al., *Hydrogen peroxide in hepatic microsomes.* Methods Enzymol, 1978. **52**: p. 342-50.

67. Macheroux, P., et al., *FAD and substrate analogs as probes for lysine N6-hydroxylase from Escherichia coli EN 222.* Eur J Biochem, 1993. **213**(3): p. 995-1002.

68. Thariath, A., et al., *Construction and biochemical characterization of recombinant cytoplasmic forms of the IucD protein (lysine:N6-hydroxylase) encoded by the pColV-K30 aerobactin gene cluster.* J Bacteriol, 1993. **175**(3): p. 589-96.

69. Jones, K.C. and D.P. Ballou, *Reactions of the 4a-hydroperoxide of liver microsomal flavin-containing monooxygenase with nucleophilic and electrophilic substrates.* J Biol Chem, 1986. **261**(6): p. 2553-9.

70. Entsch, B. and W.J. van Berkel, *Structure and mechanism of para-hydroxybenzoate hydroxylase.* FASEB J, 1995. **9**(7): p. 476-83.

71. Poulsen, L.L. and D.M. Ziegler, *The liver microsomal FAD-containing monooxygenase. Spectral characterization and kinetic studies.* J Biol Chem, 1979. **254**(14): p. 6449-55.

72. Meneely, K.M., et al., *Kinetic mechanism of ornithine hydroxylase (PvdA) from Pseudomonas aeruginosa: substrate triggering of O2 addition but not flavin reduction.* Biochemistry, 2009. **48**(20): p. 4371-6.

73. Beaty, N.B. and D.P. Ballou, *The oxidative half-reaction of liver microsomal FAD-containing monooxygenase.* J Biol Chem, 1981. **256**(9): p. 4619-25.

74. Torres Pazmino, D.E., et al., *Kinetic mechanism of phenylacetone monooxygenase from Thermobifida fusca.* Biochemistry, 2008. **47**(13): p. 4082-93.

75. Fersht, A., *Structure and mechanism in protein science: a guide to enzyme catalysis and protein folding.*, ed. A. Fersht. 1999, New York: W.H. Freeman and Company.

76. Ballou, D.P., B. Entsch, and L.J. Cole, *Dynamics involved in catalysis by single-component and two-component flavin-dependent aromatic hydroxylases.* Biochem Biophys Res Commun, 2005. **338**(1): p. 590-8.

77. Xun, L. and E.R. Sandvik, *Characterization of 4-hydroxyphenylacetate 3-hydroxylase (HpaB) of Escherichia coli as a reduced flavin adenine dinucleotide-utilizing monooxygenase.* Appl Environ Microbiol, 2000. **66**(2): p. 481-6.

78. Lobley, A., L. Whitmore, and B.A. Wallace, *DICHROWEB: an interactive website for the analysis of protein secondary structure from circular dichroism spectra.* Bioinformatics, 2002. **18**(1): p. 211-2.

79. Laemmli, U.K., *Cleavage of structural proteins during the assembly of the head of bacteriophage T4.* Nature, 1970. **227**(5259): p. 680-5.

80. Dick, S., et al., *Lysine: N6-hydroxylase: stability and interaction with ligands.* J Protein Chem, 1999. **18**(8): p. 893-903.

81. Leiros, H.K., et al., *Trypsin specificity as elucidated by LIE calculations, X-ray structures, and association constant measurements.* Protein Sci, 2004. **13**(4): p. 1056-70.

82. Alfieri, A., et al., *Revealing the moonlighting role of NADP in the structure of a flavin-containing monooxygenase.* Proc Natl Acad Sci U S A, 2008. **105**(18): p. 6572-7.

83. Malito, E., et al., *Crystal structure of a Baeyer-Villiger monooxygenase.* Proc Natl Acad Sci U S A, 2004. **101**(36): p. 13157-62.

84. Kelley, L.A. and M.J. Sternberg, *Protein structure prediction on the Web: a case study using the Phyre server.* Nat Protoc, 2009. **4**(3): p. 363-71.

85. Steennis, P.J., et al., *On the interaction of para-hydroxybenzoate hydroxylase from Pseudomonas fluorescens with halogen ions.* FEBS Lett, 1973. **36**(2): p. 177-80.

86. Gatti, D.L., et al., *The mobile flavin of 4-OH benzoate hydroxylase.* Science, 1994. **266**(5182): p. 110-4.

87. Marrone, L., M. Beecroft, and T. Viswanatha, *Lysine: N6-Hydroxylase: cofactor interaction.* Bioorganic Chemistry, 1996. **24**: p. 304 - 317.

88. Gadda, G., A. Negri, and M.S. Pilone, *Reaction of phenylglyoxal with arginine groups in D-amino-acid oxidase from Rhodotorula gracilis.* J Biol Chem, 1994. **269**(27): p. 17809-14.

89. DeLano, W.L., *Use of PYMOL as a communications tool for molecular science.*, in *Abstracts of papers of the American Chemical Society*. 2004. p. U313 - U414.